THE EFFECT OF CALCIUM LIGNOSULFONATE ON ETTRINGITE FORMATION IN CEMENT PASTE

A. Colombo (1), M. Geiker (1), H. Justnes (2, 3), R. A. Lauten (4), K. De Weerdt (1)

(1) Department of Structural Engineering, Norwegian University of Science and Technology, NTNU, Norway

(2) SINTEF Building and Infrastructure, Trondheim, Norway

(3) Department of Materials Science and Engineering, Norwegian University of Science and Technology, NTNU, Trondheim, Norway

(4) Borregaard, Sarpsborg, Norway

ABSTRACT

The effect of a softwood calcium lignosulfonate, LSs, on the ettringite formed in cement paste was investigated. Two Portland cements, mainly differing in surface area and C_3A content, were used. The effect of LSs addition time was studied, by adding either the LSs immediately with the mixing water or after 10 minutes of hydration. After 30 minutes of hydration of both cement pastes, the immediate addition of LSs caused the formation of numerous small ettringite crystals. The ettringite crystals had similar shape in pastes with and without LSs addition: cubic or cuboidal shape with length between 0.1 and 0.4 µm. These small particles caused an increase in surface area, which in turn increased the LSs adsorption by the cement paste. This could potentially lead to incompatibility issues between cement and plasticizer.

KEYWORDS

Ettringite; Hydrated surface area; Adsorption; Fresh cement paste; Lignosulfonate

1. INTRODUCTION

Water-reducers, or plasticizers, allow obtaining highly fluid concrete with low water-to-binder ratios, additionally improving the mechanical properties and the durability of the hardened concrete.

In this paper, a low-sugar softwood calcium lignosulfonate (LSs) is investigated. LSs is commonly used in concrete in the dosage of 0.25-0.40 mass % of binder. Lignosulfonates are polyelectrolytes derived from lignins in the pulping industry. Lignin can be derived from various sources of biomass, which allows producing lignosulfonates with different molecular weight and amount of functional groups, as explained by Gelardi et al. [1], amongst others.

Amongst the clinker phases, C_3A is the one with the highest hydraulic reactivity, reacting immediately upon water contact. In the presence of gypsum, the first stable hydration product from C_3A is ettringite (AFt). Ettringite forms as long as there are enough sulfate ions in solution. When gypsum is depleted, ettringite will start further reacting with the residual C_3A, forming monosulfoaluminate hydrate (AFm) [2].

The dispersing effectiveness of a superplasticizer on cementitious materials is, amongst others, a function of its degree of adsorption on the surface of cement grains and hydrates. The two main dispersing mechanisms are electrostatic repulsion and steric hindrance. The plasticizer type determines which of the two mechanisms will be dominant. During electrostatic repulsion the adsorbed plasticizer layer renders the particle surface negatively charged. As negatively charged particles approach each other, electrostatic repulsion prevents them from forming agglomerates. Additionally, when two surfaces approach close enough for their adsorbed layers to overlap, a steric force develops. This will contribute in hindering particles to get close enough to form agglomerates. The key parameters that govern the steric repulsion are the adsorption layer thickness and its conformation at the solid liquid interface

[3]. Lignosulfonate can disperse cement particles by both electrostatic repulsion and steric hindrance, as reported by Vikan [4], amongst others.

The amount of substrate surface which is covered by adsorbed polymer is referred to as surface coverage. As both major dispersion mechanisms rely on surface coverage, it will be a dominating parameter with regard to the dispersing efficiency of plasticizers. In a previous paper [5], the authors showed that the rheological behavior relates to the degree of polymer coverage of the available surface for adsorption. In particular, the achievement of high or full surface coverage was found to correspond to a drop in yield stress and viscosity of the cement paste.

The polymer is not adsorbed equally on the four main cement phases. According to Yoshioka et al. [6], a much higher adsorption occurs on aluminate and ferrite than on the silicate phases. According to Zingg et al. [7] and Plank et al. [8], the plasticizer will be adsorbed also on the cement hydrates, ettringite being the hydrate adsorbing the most.

It is known that plasticizers can cause changes in hydrates morphology, especially for ettringite. Prince et al. [9] studied a system of calcined kaolin, lime and anhydrite and found that sodium polynaphthalene sulfonate blocks the development of needle-like ettringite crystals. Instead, ettringite formed in small massive clusters. Hekal and Kishar [10] found that the size of the ettringite crystals formed in a C_3A-$CaSO_4$ system decreased as the dosage of a sodium naphthalene sulfonate-formaldehyde polycondensate increased. Cody et al. [11] synthesized ettringite in presence of a commercial lignosulfonate. They found that a large amount of ettringite formed in the form of small spherical crystals. Danner et al. [12] observed that the addition of calcium and sodium lignosulfonate led to the formation of small ettringite crystals with rounded oval shape. On the other hand, Kerui et al. [13] investigated a fly ash cement, reporting that a mixture of calcium lignosulfonate and sodium bicarbonate

caused a change in ettringite formation from a large number of tiny crystals into a limited number of large needle-like crystal particles. In conclusion, generally [9-12] plasticizers have been reported to cause the ettringite crystals to be smaller in size and to deviate from the typical needle-shape, taking a spherical or cubic morphology, except for Kerui et al. [13], who found that ettringite formed in few large needle-like crystals. However, it should be kept in mind that the results might have been influenced by the fact that lignosulfonate was combined with $NaHCO_3$.

Several studies reported that also the amount of formed hydrates might change upon plasticizer addition. Zingg [14] found that some polycarboxylate-type superplasticizers (PCE) had a limited influence on the amount of ettringite formed in Portland cements. This was confirmed by Dalas et al. [15], who found only a slight decrease in the amount of ettringite precipitated in a C_3A-$CaSO_4$ system, though its specific area was strongly increased. Hekal and Kishar [10] investigated a similar system of C_3A and $CaSO_4$ reporting that the ettringite formation was increasingly retarded in the first 24 hours of hydration as the dosage of a sodium naphthalene sulfonate-formaldehyde polycondensate increased. Lignosulfonate was, on the other hand, found to accelerate ettringite formation in cement by Bishop and Barron [16]. The amount of ettringite formed by a fly ash cement was found to increase in presence of a mixture of calcium lignosulfonate and sodium bicarbonate by Kerui et al. [13]. Danner et al. [17] investigated three different cements in combination with a calcium-lignosulfonate and reported that the initial formation of ettringite was accelerated. In conclusion, the amount of ettringite formed has both been observed to increase and decrease depending on the plasticizers used.

The aim of this paper is to understand the effect of a calcium lignosulfonate (LSs) on the formation of ettringite in Portland cement paste. Two Portland cements mainly differing in surface area and C_3A content were chosen. The effects were studied both by adding the

lignosulfonate immediately with the mixing water (IA), and by adding it after 10 minutes of hydration (DA). Changes in composition and amount of cement hydrates after 30 minutes of hydration caused by the addition of the LSs were investigated with thermogravimetric analysis (TGA) and X-ray powder diffraction (XRD). The effect of LSs on the hydrates of hardened cement was also studied with TGA after 28 days of hydration. The hydrates morphology was observed with scanning electron microscopy (SEM) after 30 minutes of hydration, and their chemical composition was analyzed with energy dispersive spectroscopy (EDS). The elemental composition of the pore solution extracted from the cement paste samples after 30 minutes of hydration was analysed with inductive coupled plasma – mass spectroscopy (ICP-MS). In addition, the effect of LSs on the solubility of the different calcium sulfates, i.e. anhydrite, hemihydrate and gypsum, was investigated by determining the soluble Ca and S by ICP-MS in calcium sulfate suspensions containing increasing LSs dosages. The adsorption isotherms and BET measurement presented in a previous paper by the same authors [18] were combined with the new results reported in the present paper. In the present paper, the authors succeeded in observing the morphology of ettringite in real cement paste with and without the LSs, and not as a pure synthesized phase. The results of this paper are connected to those discussed in a previous paper by the same authors [5], which was more focused on the effect of LSs on setting time and rheology of cement paste. The results of the present paper give further insight on the effect of LSs on the formation of cement hydrates, and thus contribute to a deeper understanding of the mechanisms behind the interactions between lignosulfonate and cement paste.

2. EXPERIMENTAL

2.1 Materials

The experiments were performed on two different cements: a CEM I 52.5 N (ANL) produced by Norcem, and a CEM I 52.5 R (CX), produced by Cemex, as defined by the European Standard EN197-1. The content of the main clinker phases of the cements quantified by XRD Rietveld, according to Le Saoût et al. [19], are given in Table 1. The chemical composition of the cements determined by XRF and the loss of ignition at 950 ºC are reported in Table 2. The particle size distribution (d_{10}, d_{50}, d_{90}), Blaine surface area, density, and BET surface area are given in Table 3.

A sugar-reduced softwood calcium lignosulfonate (LSs), produced by Borregaard, was used as plasticizer. Fractionated lignosulfonate samples with low polydispersity indices and known molecular weight were used as calibration standards for determination of molecular weight. Its weight average molecular weight (M_w), as measured with gel permeation chromatography (GPC), was 29000 g/mol and the number average molecular weight (M_n) was 2100 g/mol, giving broad molar-mass dispersity ($Đ_M$) equal to 13.8. The molar-mass dispersity, also called polydispersity index, is defined as the ratio between M_w and M_n [20]. Additional physical and chemical properties of the lignosulfonate are listed in Table 4. For the lignosulfonate used in the present investigation, the sugars were removed from the product by fermentation and resulting alcohol by distillation. The LSs was dissolved in deionised water to concentrations varying from 1 to 45 % to facilitate dosing, and the water content was included in the calculation of the water-to-binder ratio (w/b).

In order to study the effect of LSs on the solubility of calcium sulfates, anhydrite ($CaSO_4$), hemihydrate ($CaSO_4 \cdot 0.5H_2O$) and dihydrate ($CaSO_4 \cdot 2H_2O$) were used. The anhydrite, produced by Thermo Fisher, and the dihydrate, produced by Merck, were analytical grade,

while the hemihydrate, produced by VWR Chemicals, was technical grade. In order to mimic the pH of cement paste, the calcium sulfates samples were mixed with LSs solution diluted in artificial pore water. The artificial pore water was a solution of 2.1 g/l NaOH and 5.9 g/l KOH with K/Na, reaching a measured pH of 12.9. A molar ratio of 2 for K/Na is typical for a Norwegian Portland cement, see [21].

2.2 Sample preparation

About 300 g cement was mixed with deionised water and/or lignosulfonate solution in a high-shear mixer MR530 by Braun at intensity 6 obtaining a paste with w/b = 0.4. A volume of about 200 ml was obtained for all the cement pastes. In order to investigate the effect of the time of addition of lignosulfonate, two different mixing procedures were applied: immediate addition of LSs with the mixing water (IA) and delayed addition of LSs after 10 minutes of hydration (DA).

For IA, the binder was mixed with deionised water (and/or lignosulfonate diluted in deionised water) according to the procedure used by Vikan [4]: 30 seconds mixing, 5 minutes resting and scraping the mixer walls to homogenize the mix, and 1 minute mixing.

For DA, the binder and 85% of the water were mixed according to the following mixing procedure: 30 seconds mixing, 10 minutes resting and scraping the mixer walls to homogenize the paste. The delay time of 10 minutes was found to be included in the range of optimum delay times to obtain the maximum workability increase with a given plasticizer dosage [22-25]. LSs and the remaining 15% of the needed water were then added to the mix, which was mixed for 1 additional minute.

2.3 Methods

2.3.1 UV-spectroscopy

UV-spectroscopy allowed measuring the LSs concentration in the pore solution of the cement paste samples, which again allows the determination of the LSs uptake.

After mixing according to paragraph 2.2, about 35 ml paste was poured in 50 ml plastic centrifuge tubes and left to rest until the selected hydration time. The pore solution was extracted from the cement paste by centrifuging the samples in a Heraeus Megafuge 8 centrifuge by Thermo Scientific for 3 minutes at the speed of 4500 rpm. The supernatant pore solution was extracted and filtered with 0.45 µm cellulose syringe filters. The pore water was analysed with a Genesys 10S UV-spectrophotometer by Thermo Scientific. Wavelengths in the range 280-284 nm had been reported in literature to study the adsorption of lignosulfonate on cement particles [3, 4, 26-28]. After scanning at several wavelengths, 281 nm was chosen as the most suitable wavelength to analyse the samples in this study.

After centrifugation plasticizer consumed by the cement paste was determined with UV-spectroscopy at increasing hydration times (from 5 to 120 minutes hydration). It was found that, after 10 minutes of hydration, the LSs uptake reached a plateau and did not change considerably with time. 30 minutes hydration was used for determination of the adsorption isotherms.

A calibration curve was obtained measuring the absorbance of pure LSs solutions dissolved in deionised water in different concentrations. Based on the absorbance value of the pore solution extracted from the samples of cement paste, the calibration curve allowed the calculation of the amount of free plasticizer (g LS/100 g solution) in the pore solution. This amount was then related to the amount of binder in the sample (g LS/100 g binder). The LSs consumed by the investigated systems was calculated by subtracting the amount of free LSs to

the total amount of LSs initially added to the sample (also called depletion method), as displayed in equation 1:

$$LSs_{consumed} = LSs_{total} - LSs_{free} \quad (1)$$

Polymer adsorption by a solid is usually described through isotherms, in which the amount of polymer adsorbed is plotted against the total amount of polymer added to the system [29]. The shape of an isotherm is largely determined by the adsorption mechanisms. In this study, the isotherms were drawn relating the amount of LSs consumed by the cement paste to the amount of total LSs added to the sample. When expressed as mass % of binder, the amount of LSs consumed was calculated considering the actual available water in the system, i.e. the mixing water was reduced by the bound water measured with TGA (paragraph 2.3.3).

2.3.2 Solvent exchange

A solvent exchange procedure with isopropanol and petroleum ether, similar to the one suggested by Winnefeld et al. ([30]) and Lotenbach et al. ([31]), was used to stop the hydration of the cement paste. It should be noted that the method for stopping hydration of the cement paste and drying might affect the amount and the morphology of the ettringite observed [30, 31].

About 5 ml of cement paste after 30 minutes of hydration was transferred in a 50 ml centrifuge tube and centrifuged for 1 minute at 2000 rpm. The supernatant water was removed. About 40 ml of isopropanol was poured in the centrifuge tube. The tube was shaken for 30 seconds and let to rest for 5 minutes. The sample was centrifuged again for 1 minute at 2000 rpm and the supernatant liquid was removed. The solvent exchange procedure with isopropanol was repeated once, followed by a final solvent exchange with 10 ml of petroleum ether. The resulting paste was let to dry in a ventilated oven for 15 minutes at 40 ºC, and then for 2 days in a desiccator over silica gel and soda lime to minimize carbonation. After drying,

the samples were pulverized and homogenized in a porcelain mortar and stored in sealed containers in a desiccator over silica gel and soda lime until analysis.

After 6 hours of hydration, a slice of 6 mm was cut from the mid-section of the sample with an electric saw (the samples were not plastic anymore, but neither fully hardened). For this reason, the semi-hardened cement paste was crushed in a porcelain mortar and the hydration was stopped in equal manner as for the samples hydrated for 30 minutes.

A different set of samples of cement paste was let to hydrate for 28 days at 20 ºC in sealed conditions. After 28 days, a slice of 6 mm, equivalent to about 5 g of cement, was cut from the mid-section of the sample with an electric saw. The sample was crushed in a porcelain mortar until the powder passed through a 1 mm sieve. The powder was then transferred into a 125 ml plastic bottle together with 50 ml isopropanol, which was shaken for 30 seconds and let to rest for 5 minutes until solids sedimented. The isopropanol was decanted and the procedure was repeated once more. The isopropanol was then filtered off with a filtration unit connected to a water pump, using Blauband filters by Schleicher & Schuell. The sample was then flushed with 10 ml petroleum ether while still in the filtration unit, and let to rest for 5 minutes, before removing the ether by filtration in the water pump. The sample was then transferred to a watch glass and let to dry in a ventilated oven for 15 minutes at 40 ºC. After drying, the samples were stored in sealed containers in a desiccator over silica gel and soda lime until analysis. Prior to analysis, the sample was pulverized and homogenized in a porcelain mortar.

2.3.3 TGA

The thermogravimetric analysis (TGA) was performed with a Mettler Toledo TGA DSC3+ on hydrated cement paste after stopping the hydration using solvent exchange. Approximately

200 mg of cement paste powder was loaded in 600 µl alumina crucibles. The samples were heated from 40 to 900 °C at a rate of 10 °C/min while purging with 50 ml/min N_2.

It was decided to present the results in terms of mass loss % of the mass of dry binder in different temperature intervals (see Figure 7 and Table 6). The intervals selected were: interval 1, from 50 to ca. 300 °C, interval 2 from ca. 300 to ca. 500 °C, and interval 3 from ca. 500 to 900 °C. The temperature ranges could slightly vary according to the actual peak boundaries in the derivative of the thermogravimetric curve (DTG). For the samples hydrated for 28 days, the intervals slightly changed in temperature ranges: interval 1, from 50 to ca. 420 °C, interval 2 from ca. 420 to ca. 540 °C, and interval 3 from ca. 540 to 900 °C.

Interval 1 includes the mass loss corresponding to the decomposition of ettringite, calcium sulfates, and C-S-H; interval 2 consists mainly of the mass loss corresponding to the decomposition of CH; interval 3 comprises the mass losses corresponding to the decomposition of carbonates. The sum of the mass loss in the interval 1 and 2 represents the release of bound water.

The mass losses are expressed relative to the dry mass of the sample as the dry weight is assumed to be constant during the hydration. Commonly the mass at 500 °C is used as the dry mass of hydrated cement paste containing limestone [21]. However, the addition of LSs to the cement paste led to an increase in mass loss in the temperature range between 500 and 800 °C due to the decomposition of LSs. Therefore, the dry weight was calculated as the sum of the sample weight at 800 °C (w_{800}) and the mass loss due to the decomposition of limestone in the sample without LSs ($w_{ref,500} - w_{ref,800}$). For example, the mass loss in interval 1 was calculated as in equation 2:

$$\text{Mass loss Int. 1 (mass \%)} = \frac{w_{50} - w_{300}}{w_{800} + (w_{ref,500} - w_{ref,800})} * 100 \quad (2)$$

To calculate the amount of bound water in the cement paste, the mass loss in the interval from 50 to 500 ºC was considered. The amount of bound water was calculated as:

$$\text{Amount of bound water (mass \% dry weight of cement)} = \frac{w_{50}-w_{500}}{w_{800}+(w_{ref,500}-w_{ref,800})} * 100 \quad (3)$$

In order to have an approximate quantification of the maximum amount of ettringite formed after 30 minutes in the cement pastes in which 1.5 mass % of LSs was added by IA, the whole mass loss in the interval 1 (50 - ca. 300 ºC) was considered. The amount of ettringite (AFt) was calculated as:

$$\text{Amount of AFt (mass \% dry weight of cement)} = \frac{w_{50}-w_{300}}{w_{800}+(w_{ref,500}-w_{ref,800})} * \frac{M_m(AFt)}{M_m(H)} * 100 \quad (4)$$

Where M_m(AFt) and M_m(H) is the molecular mass of ettringite and water respectively.

It should be noted that in this temperature interval also C-S-H and calcium sulfate components could lose water. However, the mass loss due to C-S-H decomposition was expected to be very small as no C-S-H was not observed in these samples using SEM-EDS. The mass loss due to the release of crystalline water from the remaining calcium sulfate components present cannot be separated from the mass losses corresponding to ettringite as the TGA peaks overlap. This might lead to a slight overestimation of the amount of ettringite formed, however this is acceptable as the aim is to obtain an estimate of the potential maximum amount of ettringite.

2.3.4 XRD

The X-ray diffraction (XRD) analysis was performed using a Bruker AXS D8 Focus with a Lynxeye super speed detector operating at 40 kV and 40 mA. A CuKα source (λCuKα = 1.54 Å) with a 0.2 mm slit was used. The scan was performed between 7 and 55° 2θ with an

increment of 0.02 and a scanning speed of 0.5 s/step. Front-loading sample holders were used. The scans are used qualitatively to detect changes in crystalline phases.

2.3.5 BET of hydrated particles

The BET measurements were performed using a Flowsorb II 2300 by Micromeritics. The sample mass was about 2 g. The measurement was performed by purging the samples with nitrogen at room temperature. The initial flow of gas through the sample was stable, hence the samples were dry. Therefore, the samples were neither dried nor degassed before the measurement, in order to preserve the ettringite possibly present in the sample. The sample preparation applied in this study, similar to the one described in [32], aimed to limit destruction of hydrates such as gypsum and ettringite. The hydration was stopped with the solvent exchange procedure described in paragraph 2.3.2.

2.3.6 SEM-EDS

An ultra-high-resolution in-lens cold field emission SEM S-5500 by Hitachi was used for the scanning electron microscopy (SEM). The cement powder was dried for 2 days in a desiccator over silica gel and soda lime prior to the analysis. The powder sample was placed on a sample holder with copper tape and the excess powder was removed with a N_2 gun. A voltage of 5 kV and a current varying between 1 and 7 µA were used to observe the samples with the scanning electron microscope in secondary electron-mode (SE). The chemical composition of the samples was analyzed with energy-dispersive X-ray spectroscopy (EDS) using a Bruker XFlash detector set on a voltage of 5 kV and a current of 20 µA. The samples were coated with a 4 nm-thick layer of a platinum-palladium alloy to avoid charging of the sample during the analysis.

2.3.7 ICP-MS

Inductively-coupled plasma mass spectrometry (ICP-MS) was used to determine the elemental concentration of Al, Ca, Fe, K, Na, S and Si in the pore solution extracted from the cement paste. A triple quad Agilent 8800 by Agilent Technologies was used. The samples were filtered with the same procedure used for UV-spectroscopy (paragraph 2.3.1) and acidified by adding 1:1 by volume of 1:10 diluted HNO_3.

3 RESULTS

3.1 TGA after 30 minutes of hydration

The effect of the dosage of LSs on cement hydrates after 30 minutes of hydration was investigated with TGA. The analysis was performed on ANL and CX cement pastes with different dosages of LSs both for immediate addition (IA) and for delayed addition (DA). A maximum LSs dosage of 1.5 mass % of binder was used for the samples prepared with DA because of the extremely large setting retardation displayed by this sample, as showed in a previous paper [5]. Reference samples of neat ANL and CX without LSs were also measured. The hydration of the tested samples was stopped after 30 minutes with the solvent exchange procedure with isopropanol and petroleum ether, as described in paragraph 2.3.2. The results are displayed in Figure 1 and in Figure 2 for ANL cement and in Figure 3 and in Figure 4 for CX cement.

Several peaks could be observed: the peak at about 110 ºC and the smaller one at 240 ºC indicate the presence of AFt. The peak around 150 ºC represents the release of water from calcium sulfates (anhydrite, hemihydrate or gypsum) ($CaSO_4 \cdot xH_2O$). This peak might overlap with the one representing the decomposition of AFm, but, since no AFm was detected with XRD (see Figure 5 and Figure 6), it is assumed that this peak is only ascribable to the release of crystalline water from the calcium sulfates. The peak around 420 ºC relates to the release of

crystalline water from portlandite (CH); the ones around 610 ºC and 780 ºC represent the decomposition of carbonates ($\underline{C}$) (release of CO_2). The peaks over 500 ºC can be attributed both to the decomposition of limestone included in the used cements and, for the samples containing LSs, to the decomposition of LSs.

After 30 minutes of hydration, the TGA data for ANL cement (see Figure 1and Figure 2) shows a peak at 150 ºC corresponding to the dehydration of gypsum and hemihydrate, which is in line with the composition of the cement given in Table 1. The TGA data for CX cement after 30 minutes of hydration (see Figure 3 and Figure 4) only shows a small peak at 150 ºC, most likely associated with the hemihydrate already present in the unreacted cement (Table 1). Changes in the anhydrite content present in the CX cement (Table 1) cannot be monitored by TGA as it does not contain chemically bound water. One might expect that anhydrite and hemihydrate present in the unreacted cement would convert to gypsum upon contact with water, but that does not seem to be the case.

The mass loss was quantified with the horizontal step method applied in three temperature intervals, as described in paragraph 2.3.3. The results are shown in Figure 7 and summarized in Table 6.

From the results showed in Figure 7 and reported in Table 6, it can be observed that, for IA, the increase in LSs dosage led for both cements to an increase in the intensity of the peak corresponding to the decomposition of ettringite and a reduction in the one corresponding to the decomposition of calcium sulfate hydrates up to a LSs dosage of 1.5 mass % of binder. Similar trends were observed for both cements, even though the ettringite peak was noticeably more intense and the one of calcium sulfate hydrates less intense for CX cement compared to ANL cement. For higher LSs dosages, the increase in intensity of the ettringite peak was lower than that with 1.5 mass % of binder LSs for both cements.

346 The mass loss corresponding to the decomposition of CH did not noticeably change with
347 increasing LSs amount.

348 The mass loss corresponding to carbonates decomposition was found to increase in intensity
349 with the increase of the LSs amount, and thereby seems to include a contribution from the
350 decomposition of consumed LSs.

351 The amount of bound water (calculated according to formula 3) followed a trend similar to the
352 one of ettringite. The highest increase in amount of bound water is shown by CX cement paste
353 for IA, which agrees with the observation that, for IA, CX was found to set already after 30
354 minutes of hydration for LSs dosages over 1.0 mass % of binder.

355 In the sample of CX cement paste with 1.5 mass % of binder LSs (IA), the amount of bound
356 water resulted to be about 5 mass % of dry weight of cement, which represented the 12 % of
357 the initial mixing water (40 mass % of dry weight, since w/b = 0.4).

358 For DA, no noticeable changes in the ettringite, calcium sulfate hydrates, or CH amount were
359 observed for any of the cements. Only an increased intensity of the carbonate peak was
360 measured with increasing LSs amount.

361 **3.2 XRD**

362 The increase in the ettringite amount measured with TGA for IA was confirmed by x-ray
363 diffraction (XRD) on ANL and CX cement pastes containing 0, 0.8, 1.5 mass % of binder LSs
364 added with IA. The hydration of the cement pastes was stopped after 30 minutes with the
365 solvent exchange procedure using isopropanol and petroleum ether, as described in paragraph
366 2.3.2. The results are shown in Figure 5 and Figure 6.

367 The main peaks displayed by the XRD curves are summarized in Table 7. The peak at 2θ =
368 9.1°, representing ettringite, increases in intensity with the increase of LSs for both cements,

supporting the results found with TGA. For the ANL cement samples, clear peaks at 2θ = 11.6 º and 20.7 º are observed, representing gypsum. Whereas for CX cement samples, peaks at 2θ = 25.7 º and 31.2 º were detected and represent anhydrite. This is in line with the composition on the unhydrated cements (Table 1), where the sulfate source in CX cement is anhydrite and hemihydrate, and for ANL cement gypsum and hemihydrate, with the exception that hemihydrate was not detected in the XRD spectrum, supposedly because it dissolves very quickly. For ANL and CX cement, the peak intensities of respectively gypsum and anhydrite noticeably decreased with the LSs dosage, indicating enhanced reaction of the calcium sulfate phases upon addition of LSs. The peaks at 2θ = 12.2 º and 2θ = 24.3 º indicates C_4AF, which appeared to slightly decrease with increasing LSs dosage. The peak at 2θ = 14.9 º represents C_3S and displayed an approximately constant intensity with increasing LSs dosage in both cement pastes, which is in line with the fact that the hydration of C_3S is still very low after only 30 minutes of hydration. The peak at 2θ = 23.0 º indicates either ettringite or $CaCO_3$. This peak was found to slightly increase with the increase in LSs for both cements.

3.3 SEM

3.3.1 After 30 minutes of hydration

The morphology and size of early hydrates in presence of LSs was investigated with SEM. Pastes of both cements containing 1.5 mass % of binder LSs both for IA and DA were studied. The hydrates formed in these samples were compared to those formed in reference samples without LSs.

Figure 8 displays grains of left) ANL and right) CX cement after 30 min hydration without LSs. Both cements showed large areas of unhydrated surface and few initial hydrates. It was noted that the presence of hydrates was largest inside cavities and holes on the particles' surface. It should also be kept in mind that the presence of crystals on the surface of

anhydrous cement particles depends on the fact that the crystals, which are initially dispersed in the pore solution, land on the surface of the anhydrous cement particles when the sample is dried.

Figure 9 and Figure 10 display a typical particle of ANL and CX cement after 30 minutes of hydration, respectively, with 1.5 mass % of binder LSs mixed with IA. Large portions of the particles' surface were covered with crystals. The crystals were cubic with size between 0.1 and 0.2 μm for ANL cement, and cuboidal with length between 0.2 and 0.4 μm for CX cement (aspect-ratio varying between 1.5:1 and 4:1). For CX cement, the crystals appeared to be larger in amount than in ANL cement, being located densely on top of each other on the cement grains' surface.

When the same LSs amount was added with DA, as shown in Figure 11 and in Figure 12 for ANL and CX cement, respectively, the surfaces of particles and hydrates appeared rough and irregular, with fewer well-defined crystals than when the LSs was added with IA (see Figure 9 and Figure 10).

SEM-EDS was performed in order to analyse the chemical composition of the crystals present on the surface of unhydrated cement grains. The results from the SEM-EDS analysis of two crystals are displayed in Figure 13 and in Figure 14. It has to be noticed that the crystals turned to more rounded shapes during the scanning due to dehydration.

The SEM-EDS line scans allowed a qualitative chemical analysis of a line of points which included both the crystals and the unhydrated cement grain below them. In both cements, the results showed that, in comparison to the cement grain on which the crystals lay, the crystals were richer in Al, S and Ca, while they contained less Si.

The chemical composition of the samples was analysed by performing SEM-EDS analysis on 4 points for each object analysed. The objects analysed were both the crystals and the

underlying cement grains. The average content in Al, Si, S and Ca of 4 analysis points was calculated for both cement pastes. Al and S were used to identify the phase composing the crystals, as the crystals analysed were deposited on C_3S surfaces. The crystals were found to contain Al and S in ratio of about 1:3 in ANL cement and 1.8:3 in CX cement. The theoretical Al to S ratio in ettringite is 2:3. Considering the non-ideal conditions for SEM-EDS analysis (e.g. relief, small crystals, and charging material) and the limited number of data points, the crystals were identified as ettringite, even though the observed ratio between Al and S was lower than the theoretical one for ettringite for both cement pastes.

3.3.2 After 6 hours of hydration

The ettringite formed by pastes of the two cements without LSs was observed with SEM at final setting. The aim was to verify whether the ettringite crystals formed by pastes of the two cements without the LSs at a later stage of hydration displayed a needle-like shape and to compare them to those formed after 30 minutes of hydration.

The analysis time was after 6 hours of hydration, which corresponded to a time right before the main hydration peak determined by isothermal calorimetry, as shown in a previous paper [5]. It was assumed that, at this time of hydration, a minor amount of AFm or no AFm was present. The results are shown in Figure 15 for ANL cement paste and in Figure 16 for CX cement paste.

The particles of both cement samples without LSs were completely covered by hydrates after 6 hours of hydration. C-S-H appeared as thin needles or fibres about 0.3 µm long and about 0.05 µm wide. The C-S-H fibres embedded some ettringite crystals varying in morphology. Some ettringite crystals appeared as parallelepipeds with dimensions about 0.10x0.15 µm, while other crystals appeared more needle-like, with dimensions about 0.4x0.1 µm. Some clinker grains displayed more ettringite crystals on their surface, others less. In general, there

seems to be an indication of more ettringite crystals on the CX clinker grains compared to ANL ones, in agreement with the difference in cement composition and fineness.

The identification of ettringite and C-S-H was based on visual appearance and on the comparison to references in literature [33] and supported by SEM-EDS. Because of the high density of hydrates on the surface of unhydrated cement grains, it was difficult to analyse their chemical composition with SEM-EDS. However, the SEM-EDS analysis of the crystals visually identified as ettringite indicated that they contained Al and S, while the crystals identified as C-S-H appeared to be richer in Ca and Si.

3.4 BET

The BET surface area was measured for ANL and CX cement pastes with varying LSs amounts after 30 minutes of hydration. The hydration was stopped by solvent exchange after 30 minutes. The results are shown in Figure 17.

For both cements the surface area was found to increase as the dosage of plasticizer added to the cement paste increased. The increase in surface area was noticeably larger for CX than for ANL cement, and for IA compared to DA, corresponding to more AFt formed.

3.5 Adsorption isotherms

3.5.1 Cement pastes

The adsorption isotherms obtained for ANL and CX cement pastes were achieved by plotting the amount of consumed polymer versus the total amount of polymer added after 30 minutes of hydration. The tested dosages are given in Table 5. The LSs was added to the cement paste either immediately together with the mixing water (IA), or after 10 minutes of hydration (DA). Note that the adsorption isotherm obtained for CX cement for IA could only be measured up to 1.0 mass % of binder LSs. At higher dosages it was not possible to extract pore water as the paste had hardened after 30 minutes of hydration. The results and their fits

according to the Langmuir model [29] are presented as mass % of binder in Figure 18 a, and relative to the BET hydrated specific surface area (Table 3) available for adsorption in Figure 18 b.

Figure 18 a shows that, for DA, an adsorption plateau was found for both cements. At high LSs dosage the isotherms obtained for DA also displayed a considerably lower amount of LSs consumed by the cement pastes compared to the isotherms obtained for IA. According to the theory reported in [29], an adsorption plateau is achieved when full monolayer surface coverage is reached. Therefore, for DA, the LSs consumption was considered to be mainly due to monolayer surface adsorption on the cement particles and hydrates, as reported in a previous paper [18].

For IA, no adsorption plateau could be detected within the tested range, neither for ANL nor for CX cement. The isotherms' shape indicated a continuous LSs uptake as more LSs was added to the mix.

In Figure 18 b the consumed LSs was expressed relative to the available surface after 30 minutes of hydration. The adsorption isotherms of CX cement paste for IA and DA nearly coincided, both reaching an adsorption plateau. As found in [18], this indicates that the high LSs consumption by CX cement paste for IA was mainly due to monolayer surface adsorption on the large specific surface area caused by the additional ettringite formed.

For ANL cement, the amount of ettringite formed, and in turn the surface area, increased only moderately compared to CX cement (see Figure 17). Thus, as concluded in [18], surface adsorption could not entirely explain the measured LSs consumption. Therefore, for IA, other polymer consumption mechanisms, still to be determined, might have played a role in consuming the LSs in ANL cement paste.

3.5.2 Calcium sulfates

CX cement paste formed a larger amount of ettringite for IA compared to ANL cement paste. One of the differences between CX and ANL cement is the calcium sulfate source present, i.e. CX contains mainly anhydrite whereas ANL contains mainly gypsum (see Table 1). The difference in the amount of ettringite formed in both cement pastes might be related to the differences in the dissolution of the calcium sulfates i.e. enhanced dissolution of anhydrite compared to gypsum in the presence of LSs might have led to a higher amount of ettringite formed. In order to verify this, the interaction between the LSs and gypsum, hemihydrate and anhydrite was investigated. Adsorption isotherms were measured for anhydrite ($CaSO_4$), hemihydrate ($CaSO_4 \cdot 0.5H_2O$) and gypsum ($CaSO_4 \cdot 2H_2O$). The samples had water-to-powder ratio 1.0 and they were analysed 30 minutes after mixing. The results are displayed in Figure 19 with unit a) mass % of solid and b) g LSs / m^2 unhydrated surface. The isotherms of ANL for IA are also shown as reference.

Figure 19 a shows that the adsorption isotherms of the three different calcium sulfates reached a plateau, which corresponds to monolayer surface saturation. The influence of the surface area was eliminated by normalizing the adsorption isotherms obtained by the BET surface area of each calcium sulfate. The results shown in Figure 19 b display that the higher LSs consumption of anhydrite was due to its higher surface area. Hemihydrate still showed a LSs consumption slightly higher than gypsum and anhydrite. Even when taking into account a hypothetical 30 % error in the BET results, the trends shown in Figure 19 b did not noticeably change. The amount of LSs consumed by the calcium sulfates was, however, noticeably lower than the one of ANL cement for IA (which was similar to that of CX cement).

3.6 ICP-MS

The elemental concentration of Al, Ca, Fe, Si and S in the pore solutions extracted from ANL and CX cement pastes after 30 minutes of hydration was determined with ICP-MS. The

cement pastes contained 0.8 and 1.5 mass % of binder LSs added either with IA and DA. Additionally, a reference sample without LSs was measured. Moreover, the content in Al, Ca, Fe, Si and S was also measured for two LSs solutions dissolved in artificial pore water at concentrations corresponding to those used in cement pastes (see Table 8). The artificial pore water composition is described in paragraph 2.1. The results from ICP-MS are shown in Figure 20 and reported in Table 8.

The samples mixed with DA showed an increase in Al, Fe and Si concentration dissolved in the pore solution as the LSs dosage increased. The increase was considerably larger for ANL cement than for CX cement. Only minor increases were measured for the samples mixed with IA. Moreover, except for CX cement for DA, the concentration of S and Ca appeared to be rather constant with increasing LSs dosage, in spite of the increased amount of these elements added by the increasing amount of LSs.

In order to investigate the effect of increasing LSs dosages on the solubility of the sulfates present in the cement pastes, the elemental concentration of Ca and S in the pore solution extracted from anhydrite, hemihydrate, and gypsum slurries after 30 minutes of hydration was determined with ICP-MS. The LSs dosages tested were 0.2, 0.4, 0.8 and 1.5 mass % of binder LSs added with IA. Additionally, a reference sample without LSs was measured. Moreover, the content in Ca and S was also measured for two LSs solutions dissolved in artificial pore water (see Table 9). The artificial pore water composition is described in paragraph 2.1.The results from ICP-MS are shown in Figure 21 and reported in Table 9.

The results, shown in Figure 21, highlight that, for LSs dosages between 0 and around 0.4 mass % of binder LSs, the trend of the content in Ca and S deviates from the one observed for higher LSs dosages. As shown by the isotherms in Figure 19, with LSs dosages under about 0.4 mass % of binder, all the samples were in a highly dynamic stage and far from reaching a

constant level of surface adsorption. For this reason, the authors decided to focus on the values of Ca and S concentrations obtained for LSs dosages higher than about 0.4 mass % of binder. The content in Ca and S was found to be nearly independent of the LSs dosage for anhydrite and hemihydrate, while for gypsum it increased slightly as the LSs dosage increased. However, the increase was less than the Ca and S provided by the additional LSs.

3.7 TGA after 28 days of hydration

The effect of increasing the LSs dosage on the hydrates formed in hardened cement paste were investigated with TGA. The analysis was performed on ANL and CX cement pastes after 28 days of sealed curing at 20 ºC containing different dosages of LSs both for IA and DA. A reference sample of neat ANL and CX without LSs was also measured. The hydration of the tested samples was stopped after 28 days with the solvent exchange procedure with isopropanol and petroleum ether, as described in paragraph 2.3.2. The results are displayed in Figure 22.

The peak at about 125 ºC and the smaller one at 270 ºC indicate the presence of AFt. The peak around 170 ºC in this case represents most likely the decomposition of AFm, since it can be expected that, after 28 days of hydration, the sulfates are depleted. The peak around 480 ºC shows the decomposition of portlandite (CH). Note that C-S-H loses water over the entire temperature range from 50 to 600 ºC, with a main weight loss coinciding with the first ettringite peak just above 100 ºC. The peaks over 600 ºC represent the decomposition of carbonates (C$\underline{C}$). These can be attributed to the decomposition of limestone included in the used cements and, for the samples containing LSs, to the decomposition of LSs.

The peaks corresponding to ettringite and to, most likely, AFm strongly overlapped for most samples. It was therefore difficult to quantify the amount of these phases. Hence it was decided to present the results in terms of mass loss % of the mass of dry binder in different

temperature intervals, as described in paragraph 2.3.3. The results are shown in Figure 23 and summarized in Table 10.

From the results shown in Figure 23 and reported in Table 10, it can be observed that, variations in the LSs dosage and time of addition (IA vs. DA), in general, led to little or no differences in mass loss % in the range comprising the AFt decomposition. For IA, there is an indication that the increase in LSs dosage for both cements led to a slight increase in the mass loss measured in interval 1 (AFt, AFm, C-S-H). As expected, the mass loss due to the decomposition of carbonates increased when more LSs was present in the mix. For ANL cement, the DA of 1.5 mass % of binder LSs caused the cement not to harden even after 28 days of hydration. For this reason the data of this sample is not showed in Figure 23 and is reported in brackets in Table 10.

4 DISCUSSION

4.1 Effect of LSs on ettringite formation in fresh cement paste

4.1.1 Ettringite amount

As displayed in Figure 1 and Figure 3, when LSs was added to the cement pastes with IA, a higher amount of ettringite was formed after 30 minutes in both cements compared to the sample without LSs, up to a threshold LSs dosage of 1.5 mass % of binder. With equal LSs dosage, a larger amount of ettringite is observed in CX cement paste compared to ANL cement paste, which might have been influenced by the larger amount of C_3A and the higher fineness of CX cement compared to ANL cement.

A higher amount of ettringite crystals in CX cement paste when LSs was added with IA could also be observed with SEM, as shown in Figure 9 and Figure 10. The ettringite morphology will be discussed more in detail in paragraph 4.1.2.

With 1.5 mass % of binder LSs added with IA, the amount of ettringite calculated according to Equation 4 was about 8 and 14 mass % of the dry weight of cement for ANL and CX cement pastes, respectively, after 30 minutes of hydration. These amounts of ettringite appear feasible when compared to other references in literature [21, 34], taking into account possible differences due to the different materials used and time of analysis.

Theoretically, the maximum amount of ettringite that can form in a cementitious system is limited either by the amount of Al_2O_3 or by the amount of SO_3 available. The amount of ettringite that theoretically can form can be calculated with the following formulas, where M_m is the molar mass:

$$\text{Amount of AFt} = Al_2O_3 \text{ amount} \cdot \frac{\text{Mm (AFt)}}{\text{Mm } (Al_2O_3)} \quad (5)$$

$$\text{Amount of AFt} = SO_3 \text{ amount} \cdot \frac{\text{Mm (AFt)}}{\text{Mm } (SO_3)} \quad (6)$$

Knowing the amount of Al_2O_3 and SO_3 available, the theoretical amount of ettringite was calculated. This amount was then compared to the amount of ettringite measured with TGA.

The Al_2O_3 amount was calculated only considering the aluminates contained in C_3A, since it was assumed that C_4AF only slightly reacted after 30 minutes of hydration. This resulted in 0.8 and 2.7 mass % Al_2O_3 in ANL and CX cement, respectively. The maximum amount of ettringite that could have formed with this amount of Al_2O_3 is 11 and 35 mass % of solid, respectively. These values are higher than those measured with TGA (8 and 14 mass % of solid for ANL and CX cement, respectively), therefore the alumina content appears not to be a limiting factor for the formation of ettringite.

The amount of SO_3 present in the calcium sulphates, as measured with XRD Rietveld, was 2.0 and 3.2 mass % of solid in ANL and CX cements, respectively. The maximum amount of ettringite that could have formed with this amount of SO_3 is 11 and 18 mass % of solid,

607 respectively. When these values are compared with the amount of ettringite formed in the
608 system as measured with TGA (8 and 14 mass % of solid for ANL and CX cement,
609 respectively), it can be noticed that neither the SO_3 content appears to be a limiting factor for
610 the formation of ettringite.

611 Finally, the LSs molecule contains sulfonate groups, which might replace the sulfates and
612 enter in the ettringite structure. Indeed, the possible replacement of the sulfates coming from
613 the calcium sulfates with the sulfonate groups contained in the LSs molecule, forming
614 intercalated calcium aluminate hydrates, was highlighted by Stöber and Pöllmann [35, 36]. In
615 the present paper, the highest amount of ettringite was formed in CX cement paste with 1.5
616 mass % of binder LSs for IA. This amount was found to be in the same range as the calculated
617 amount of ettringite based on the amount of available sulfates considering that not all the
618 sulfates were consumed after 30 minutes of hydration (14% vs. 20%). In addition, the
619 inclusion of elements or molecules in the ettringite structure would have most likely caused a
620 shift in the peaks representing ettringite in the XRD spectrum, which was not observed in the
621 samples analysed. Therefore, the intercalation of the sulfonate groups of the LSs appeared to
622 be a minor mechanism, if present at all.

623 In conclusion, the amount of ettringite measured by TGA was large, but feasible when
624 compared with literature. In the sample where the largest amount of ettringite formed, enough
625 aluminates and sulfates were available to form the entire amount of ettringite. Therefore,
626 mechanisms such as intercalation of sulfonate groups from the LSs molecule in the ettringite
627 structure seemed minor, if present at all.

628 **4.1.2 Ettringite morphology**

629 ANL and CX cement paste with 1.5 mass % of binder LSs added either with IA or with DA
630 where hydration was stopped after 30 minutes were studied with SEM in order to investigate

631 possible changes in hydrates morphology caused by the addition of LSs. The results were
632 compared to those obtained for pastes of the two cements without LSs. After 30 minutes of
633 hydration, ANL and CX cement grains appeared to be partially covered by crystals, identified
634 as ettringite with EDS (Figure 13 and Figure 14). The degree of coverage and the crystals'
635 size varied according to the presence of LSs and to its addition method: considerably fewer of
636 the smaller crystals could be observed in the samples of cement paste where no LSs was
637 added and in those where LSs was added with DA, compared to those where LSs added with
638 IA.

639 Several studies in literature found that plasticizers can change the morphology of ettringite
640 from the typical needle-like structure, to a more round or cubic one [9-12]. In partial
641 disagreement, Kerui et al. [13] found that the shape of the ettringite crystals was changed
642 from numerous small needles to few large needle-like crystals. Indeed, as observed by Shi et
643 al. [37] and hypothesized by Dalas et al. [15], superplasticizers can inhibit ettringite growth
644 by adsorbing on their surface. The crystal shape will therefore depend on the preferred surface
645 for adsorption. In the present study, the ettringite is visually observed in a real cement system
646 and not as a pure synthesized phase. The crystals observed for the two cements appeared of
647 different size and shape: cubic with size between 0.1 and 0.2 μm for ANL cement (Figure 9),
648 and with cuboidal shape with length between 0.2 and 0.4 μm for CX cement (aspect-ratio
649 varying between 1.5:1 and 4:1) (Figure 10).

650 When comparing samples of the same cement containing no LSs or 1.5 mass % of binder LSs
651 added with IA or with DA after 30 minutes of hydration, it can be noticed that the crystals of
652 ettringite displayed a similar cubic or cuboidal shape for all samples. It can be therefore
653 concluded that, after 30 minutes of hydration, the addition of LSs did not lead to changes in
654 ettringite shape for the cements analysed in this study.

Finally, ANL and CX cement paste without LSs were investigated with SEM after 6 hours of hydration. The aim was to verify whether the ettringite crystals formed by pastes of the two cements without the LSs at a later stage of hydration displayed a needle-like shape. The time of analysis corresponded to a time right before the main hydration peak determined by isothermal calorimetry, as shown in a previous paper [5], when the ettringite crystals were expected to be fully developed. The results (Figure 15 and Figure 16) displayed no major difference in ettringite morphology between the samples with 1.5 mass % of binder LSs added with IA hydrated for 30 minutes and those without LSs hydrated for 6 hours, and between the two cements. Indeed, in both systems the ettringite crystals appeared with a compact and cuboidal shape instead of the expected needle-like shape.

In conclusion, for the system analysed in this paper, no changes in the morphology of the ettringite crystals appeared to be caused by the LSs addition. These results do not fully agree with what found by other studies in literature [9-13]. This might be connected to the analytical technique used and to potential difference in the behaviour of synthetic ettringite crystals and ettringite in a hydrating cement paste.

4.2 Effect of LSs on the solubility of cement phases and calcium sulfates

The LSs used for the experiments reported in this paper is particularly rich in Ca and S (see Table 8).

Increasing dosages of LSs led to an increased concentration of Al, Fe, and Si in the pore solution of ANL and CX cement pastes (Figure 21), as shown from the ICP-MS results (Table 8). The concentration of these elements was particularly pronounced for DA. For DA, the LSs addition did not change the amount nor the type of hydrates formed by the cement pastes. The higher concentration of Al, Fe and Si relates to the dissolution of the cement phases and potentially to complexation of these elements by LSs, as mentioned by Caruso et al. [38].

679 The higher amount of ettringite formed in the CX cement might be due to a higher dissolution
680 of the anhydrite present in CX compared to the dissolution of gypsum present in ANL. In
681 order to verify this or rule this out, the content in Ca and S of the pore solution extracted from
682 gypsum, hemihydrate and anhydrite slurries containing increasing LSs dosages was measured.
683 For LSs dosages higher than about 0.4 mass % of binder, the LSs adsorption by all the
684 calcium sulfates was constant and reached a plateau, as shown by Figure 19. Therefore, when
685 more LSs was added in the solution, one would expect the concentration in Ca and S to
686 increase, as LSs is rich in both elements. However, as the LSs dosage increased, the calcium
687 sulfates showed a different behaviour: the content in Ca and S was found to be nearly constant
688 in the pore solutions extracted from anhydrite and hemihydrate, while it increased in the pore
689 solution of gypsum. However, the increase in Ca and S content was lower than it would be
690 expected from the added LSs (Table 9). These results indicate that the LSs might even
691 suppress the dissolution of gypsum, anhydrite and hemihydrate after 30 minutes of hydration.

692 In conclusion, for IA, the dissolution of gypsum, hemihydrate and anhydrite was found not to
693 be enhanced upon LSs addition. Therefore, it appears that the large increase in ettringite
694 formed was not due to an increased dissolution of the calcium sulfates.

695 The only remaining option to explain the enhanced ettringite formation is changes in the C_3A
696 reaction. When LSs is added with DA, the mixing water interacts with the clinker surface and
697 slows down the reaction of the clinker phases during the dormant period. The SEM
698 investigation of the samples where LSs was added with DA showed clinker particles with
699 many intact surfaces and very few signs of dissolution. One could imagine the formation of a
700 thin hydrate layer on the clinker surface which prevents further reaction. However when LSs
701 is added with the mixing water (IA), this hypothetical protective layer is disrupted and the
702 reaction of the C_3A is enhanced resulting in additional ettringite formation. Craters after C_3A
703 parts of the clinker grains were observed by SEM for the samples where the LSs was added

704 with IA, indicating accelerated reaction. In conclusion the enhanced ettringite formation is
705 due to accelerated C_3A reaction caused by the LSs in the mixing water.

706 **4.3 On the surface area and LSs consumption by cement paste**

707 In a previous article [18], the increase in the amount of ettringite formed in cement paste after
708 30 minutes of hydration was found to correspond to an increase in the hydrated surface area,
709 as shown in Figure 24. The increase in surface area was larger when the LSs was mixed with
710 IA and for CX cement.

711 As shown in Figure 1 and in Figure 3, a difference in amount of ettringite formed was found
712 between IA and DA with the same LSs dosage for pastes of both cements. This led to a
713 difference in surface area between IA and DA, especially for CX cement (Figure 24). This
714 caused, in turn, a difference in LSs consumption for monolayer adsorption between IA and
715 DA (Figure 18 a).

716 The amount of LSs that could potentially adsorb in a monolayer on the additional amount of
717 ettringite formed for IA was calculated. The following assumptions were made:

718 - The ettringite is characterized by a density of 1778 kg/m^3 [39], a cubic shape, and an
719 average size of 0.15 µm for ANL cement and 0.3 µm for CX cement;
720 - The entire ettringite surface area is available for polymer adsorption;
721 - The molecular footprint of LSs is 27.5 nm^2 for both cements. This value is an average
722 of the molecular footprints of the two cements, as calculated in a previous paper [18]
723 based on the amount of LSs adsorbed on the cement surface at the plateau value in the
724 adsorption isotherms.

725 The calculated amount of consumed LSs was compared to the difference in consumed LSs
726 amount experimentally measured between the sample mixed with IA and the one mixed with
727 DA at the LSs dosages of 0.8 and 1.5 mass % of binder (Table 11). The calculated ettringite

amounts were found to be lower than the measured ones for all the samples. However, for CX cement, the calculated amount was relatively close to the measured amount, also taking into account the error connected to the approximations made.

These results confirm that, for CX cement, the difference in LSs consumption between IA and DA appears to mainly be due to the additional surface available for adsorption given by the increased ettringite amount formed for IA. On the contrary, for ANL cement, the difference in LSs consumption between IA and DA cannot be due solely to the additional surface offered by the increased ettringite formed for IA.

4.4 Impact of the increased amount of ettringite on setting time and rheology of cement paste

As investigated in a previous paper [5], the increased formation of ettringite seems to have an impact on the properties of fresh cement paste, in particular on setting time and rheology. The following aspects will be separately discussed in the following paragraphs.

4.4.1 On the setting time of cement paste

In a previous paper [5] it was found that the setting retardation was directly correlated to the amount of free LSs in the pore solution. In the samples which formed the higher amounts of ettringite (IA), the increased LSs adsorption caused by the additional surface area reduced the amount of free LSs in the pore solution compared to DA for the same LSs dosage. This was reflected in a lower setting retardation for IA compared to DA for the same LSs dosage. In addition, the retardation appeared to be less sensitive to small variations in dosing for IA than for DA, i.e. the system was more robust for IA. Small variations in the dosing of the LSs with DA led to large differences in retardation: the same LSs dosage of 0.4 mass % of binder caused an increase in setting retardation of 21 and 11 hours for ANL and CX cement respectively, when compared to the setting retardation caused by the same LSs dosage added

752 with IA. This severe delay of setting can be a source of incompatibility between cement and
753 plasticizer, as described by Marchon and Flatt [40].

754 ### 4.4.2 On the rheology of cement paste

755 The presence of numerous ettringite crystals on the surface of unhydrated cement grains, as
756 observed in the present paper, could change the workability of the cement paste. The
757 increased formation of ettringite led to early stiffening of the cement paste, reduced
758 workability until potential rapid set, as measured in a previous paper [5] for CX cement with
759 1.5 mass % of binder LSs added with IA. This is a form of incompatibility between cement
760 and plasticizer, as described by Marchon and Flatt [40].

761 ## 4.5 Effect of LSs on the hydrates of hardened cement paste

762 In light of the differences in amount of ettringite in fresh cement paste caused by the addition
763 of LSs, the effect of LSs on the hydrates of 28 days-old cement were also investigated.

764 From the TGA results shown in Figure 23 and reported in Table 10, it can be observed that, in
765 all intervals, few or no differences in mass loss could be observed; neither between samples
766 containing different LSs amounts, nor between the samples prepared with IA and those
767 prepared with DA. The most noticeable change, even though still of limited entity in a general
768 scale, was observed for IA, where the increase in LSs dosage led for both cements to a slight
769 increase in the mass loss measured in interval 1 (AFt, AFm, C-S-H). In particular, the
770 intensity of the peak corresponding to the decomposition of ettringite was found to increase
771 slightly with the LSs dosage, especially for ANL cement.

772 In conclusion, the addition of LSs and its addition time seemed not to play a major role in
773 type and amount of hydrates formed in ANL and CX cement pastes after 28 days of
774 hydration. For DA, the addition of a high LSs dosage (compared to the dosages normally used

775 in practice), was found to cause lack of hardening in ANL cement even after 28 days of
776 hydration.

777 **5 CONCLUSIONS**

778 The aim of this paper was to investigate the effect of varying dosages of a softwood calcium
779 lignosulfonate (LSs) on the amount and morphology of ettringite formed in Portland cement
780 paste. Two Portland cements, CX and ANL, mainly differing in surface area and C_3A content
781 were chosen; CX had higher surface area and C_3A content than ANL. The influence of two
782 different LSs addition methods was investigated. The LSs was either added immediately to
783 the cement with the mixing water (IA), or after 10 minutes of hydration (DA). The following
784 conclusions are drawn:

785 Immediate addition (IA) of LSs to the cement pastes led to a considerable increase in the
786 amount of ettringite formed compared to pastes of the same cements without LSs. Delayed
787 addition (DA) of LSs did not affect the amount of ettringite formed.

788 For the systems analyzed in this paper, no changes in the morphology of the ettringite crystals
789 appeared to be caused by LSs addition.

790 SEM imaging allowed observing the finely dispersed ettringite crystals in the cement paste. In
791 case of immediate addition (IA) of LSs, the ettringite shape was cubic with size between 0.1
792 and 0.2 μm for ANL cement, and cuboidal with length between 0.2 and 0.4 μm for CX
793 cement (aspect-ratio varying between 1.5:1 and 4:1).

794 The study of pure calcium sulfate systems indicated that the large amount of ettringite formed
795 upon LSs addition with IA was not due to an increased dissolution of the calcium sulfates.
796 The increased amount of ettringite is due to enhanced C_3A reaction taking place when LSs is
797 added immediately with the mixing water (IA).

The presence of numerous small ettringite crystals on the surface of unhydrated cement grains upon LSs addition with IA led to an increase in plasticizer adsorption. This renders the system more robust, i.e. less sensitive to variations in dosing, regarding retardation and slump loss compared to DA. However, the large amount of crystals might potentially cause incompatibility problems due to early stiffening.

After 28 days of hydration, no noticeable effect of LSs addition and of its addition time on the amount of hydrates formed was observed, despite the large differences in the amount of ettringite formed after 30 minutes.

6 ACKNOWLEDGEMENTS

The authors wish to acknowledge the Norwegian Research Council (NFR 225358/O30) and Borregaard AS, Norway, for financing this research work. Gwenn Le Saoût and Nathalie Azema, Ecole des Mines d'Ales, France, are also acknowledged for the helpful discussions. Verner Håkonsen, NTNU, Norway, is acknowledged for performing the SEM-EDS analysis. Syverin Lierhagen, NTNU, is acknowledged for performing the ICP-MS analysis. Irene Bragstad, SINTEF, Norway, is acknowledged for performing the BET particle surface measurements.

7 REFERENCES

[1] G. Gelardi, S. Mantellato, D. Marchon, M. Palacios, A.B. Eberhardt, R.J. Flatt, 9 - Chemistry of chemical admixtures, Science and Technology of Concrete Admixtures, Woodhead Publishing2016, pp. 149-218.
[2] J. Bensted, P. Barnes, Structure and performance of cements, Taylor & Francis2002.
[3] Y.F. Houst, P. Bowen, F. Perche, A. Kauppi, P. Borget, L. Galmiche, J.-F. Le Meins, F. Lafuma, R.J. Flatt, I. Schober, P.F.G. Banfill, D.S. Swift, B.O. Myrvold, B.G. Petersen, K. Reknes, Design and function of novel superplasticizers for more durable high performance concrete (superplast project), Cement and Concrete Research, 38 (2008) 1197-1209.
[4] H. Vikan, Rheology and reactivity of cementitious binders with plasticizers, Department of Materials Science and Engineering, NTNU Trondheim, 2005.
[5] A. Colombo, M.R. Geiker, H. Justnes, R.A. Lauten, K. De Weerdt, On the effect of calcium lignosulfonate on the rheology and setting time of cement paste, Cement and Concrete Research, 100 (2017) 435-444.

[6] K. Yoshioka, E.-i. Tazawa, K. Kawai, T. Enohata, Adsorption characteristics of superplasticizers on cement component minerals, Cement and Concrete Research, 32 (2002) 1507-1513.
[7] A. Zingg, F. Winnefeld, L. Holzer, J. Pakush, S. Becker, L. Gauckler, Adsorption of polyelectrolytes and its influence on the rheology, zeta potential, and microstructure of various cement and hydrate phases, Journal of Colloid and Interface Science, 323 (2008) 301-312.
[8] J. Plank, P. Chatziagorastou, C. Hirsch, New model describing distribution of adsorbed superplasticizer on the surface of hydrating cement grain, Jianzhu Cailiao Xuebao, 10 (2007) 7-13.
[9] W. Prince, M. Edwards-Lajnef, P.C. Aïtcin, Interaction between ettringite and a polynaphthalene sulfonate superplasticizer in a cementitious paste, Cement and Concrete Research, 32 (2002) 79-85.
[10] E.E. Hekal, E.A. Kishar, Effect of sodium salt of naphthalene-formaldehyde polycondensate on ettringite formation, Cement and Concrete Research, 29 (1999) 1535-1540.
[11] A.M. Cody, H. Lee, R.D. Cody, P.G. Spry, The effects of chemical environment on the nucleation, growth, and stability of ettringite [Ca3Al(OH)6]2(SO4)3·26H2O, Cement and Concrete Research, 34 (2004) 869-881.
[12] T. Danner, H. Justnes, M. Geiker, R.A. Lauten, Early hydration of C3A–gypsum pastes with Ca- and Na-lignosulfonate, Cement and Concrete Research, 79 (2016) 333-343.
[13] Y. Kerui, Z. Caiwen, L. Zhigang, The influence of calcium lignosulphonate–sodium bicarbonate on the status of ettringite crystallization in fly ash cement paste, Cement and Concrete Research, 32 (2002) 51-56.
[14] A. Zingg, Cement-superplasticizer interaction: link between macroscopic phenomena and microstructural data on the early cement hydration, Swiss Federal Institute of Technology Zurich, 2008.
[15] F. Dalas, S. Pourchet, D. Rinaldi, A. Nonat, S. Sabio, M. Mosquet, Modification of the rate of formation and surface area of ettringite by polycarboxylate ether superplasticizers during early C3A–CaSO4 hydration, Cement and Concrete Research, 69 (2015) 105-113.
[16] M. Bishop, B.A. R., Cement Hydration Inhibition with Sucrose, Tartaric Acid, and Lignosulfonate: Analytical and Spectroscopic Study, Industrial & Engineering Chemistry Research, 45 (2006) 7042-7049.
[17] T. Danner, H. Justnes, M. Geiker, R.A. Lauten, Phase changes during the early hydration of Portland cement with Ca-lignosulfonates, Cement and Concrete Research, 69 (2015) 50-60.
[18] A. Colombo, M. Geiker, H. Justnes, R.A. Lauten, K. De Weerdt, On the mechanisms of consumption of calcium lignosulfonate by cement paste, Cement and Concrete Research, (2016, In review).
[19] G. Le Saoût, V. Kocaba, K. Scrivener, Application of the Rietveld method to the analysis of anhydrous cement, Cement and Concrete Research, 41 (2011) 133-148.
[20] R.G. Gilbert, M. Hess, A.D. Jenkins, R.G. Jones, P. Kratochvil, R.F.T. Stepto, Dispesity in polymer science, Pure applied chemistry, 81 (2009) 351-353.
[21] K. De Weerdt, M.B. Haha, G. Le Saout, K.O. Kjellsen, H. Justnes, B. Lothenbach, Hydration mechanisms of ternary Portland cements containing limestone powder and fly ash, Cement and Concrete Research, 41 (2011) 279-291.
[22] J. Hot, Influence des polymères de type superplastifiants et agents entraineurs d'air sur la viscosité macroscopique des matériaux cimentaires, Université Paris-Est, Paris, 2013.
[23] I. Aiad, Influence of time addition of superplasticizers on the rheological properties of fresh cement pastes, Cement and Concrete Research, 33 (2003) 1229-1234.
[24] G. Chiocchio, A.E. Paolini, Optimum time for adding superplasticizer to Portland cement pastes, Cement and Concrete Research, 15 (1985) 901-908.
[25] K.-C. Hsu, J.-J. Chiu, S.-D. Chen, Y.-C. Tseng, Effect of addition time of a superplasticizer on cement adsorption and on concrete workability, Cement and Concrete Composites, 21 (1999) 425-430.
[26] F. Perche, Adsorption de Polycarboxylates et de Lignosulfonates sur Poudre modele et Ciments, École Polytechnique Federale de Lausanne, 2004.
[27] K.R. Ratinac, O.C. Standard, P.J. Bryant, Lignosulfonate adsorption and stabilization of lead zirconate titanate in aqueous suspension, Journal of Colloid and Interface Science, 273 (2004) 442-454.

[28] H. Uchikawa, S. Hanehara, T. Shirasaka, D. Sawaki, Effect of admixture on hydration of cement, adsorptive behaviour of admixture and fluidity and setting of fresh cement paste, Cement and Concrete Research, 22 (1992) 1115-1129.
[29] P.C. Hiemenz, R. Rajagopalan, Principles of colloid and surface chemistry, Taylor & Francis Group1997.
[30] F. Winnefeld, A. Schoeler, B. Lothenbach, Sample preparation, in: K. Scrivener (Ed.) A practical guide to microstructural analysis of cementitious materials, CRC press2016.
[31] B. Lothenbach, P. Durdzinski, K. De Weerdt, Thermogravimetric analysis, A Practical Guide to Microstructural Analysis of Cementitious Materials, CRC press2016.
[32] S. Mantellato, M. Palacios, R.J. Flatt, Impact of sample preparation on the specific surface area of synthetic ettringite, Cement and Concrete Research, 86 (2016) 20-28.
[33] A. Bazzoni, Study of early hydration mechanisms of cement by means of electron microscopy, École Polytechnique Fédérale de Lausanne, Lausanne, 2014.
[34] K.L. Scrivener, T. Füllmann, E. Gallucci, G. Walenta, E. Bermejo, Quantitative study of Portland cement hydration by X-ray diffraction/Rietveld analysis and independent methods, Cement and Concrete Research, 34 (2004) 1541-1547.
[35] S. Stöber, H. Pöllmann, Basic investigations on the crystal chemistry of sulfonate containing AFm-phases, 11th International Congress on the Chemistry of CementDurban, South Africa, 2003.
[36] S. Stöber, H. Pöllmann, Crystalchemistry of organic sulfonates used as cement additives, Materials Science Forum, 278-281 (1998) 904-908.
[37] C. Shi, G. Zhang, T. He, Y. Li, Effects of superplasticizers on the stability and morphology of ettringite, Construction and Building Materials, 112 (2016) 261-266.
[38] F. Caruso, S. Mantellato, M. Palacios, R.J. Flatt, ICP-OES method for the characterization of cement pore solutions and their modification by polycarboxylate-based superplasticizers, Cement and Concrete Research, 91 (2017) 52-60.
[39] M. Balonis, F.P. Glasser, The density of cement phases, Cement and Concrete Research, 39 (2009) 733-739.
[40] D. Marchon, R.J. Flatt, 12 - Impact of chemical admixtures on cement hydration, Science and Technology of Concrete Admixtures, Woodhead Publishing2016, pp. 279-304.

Notation

ANL	Anlegg cement (CEM I 52.5 N)
CX	Cemex cement (CEM I 52.5 R)
$C\underline{S}H_x$	Calcium sulfate hydrates
$\underline{C}$	Carbonates (contained in $CaCO_3$ and in the LSs)
DA	delayed addition of plasticizer (10 min)
IA	immediate addition of plasticizer
LSs	softwood low-sugar Ca-lignosulfonate
OPC	ordinary Portland cement

w/b	water-binder ratio
-COOH	carboxyl group
φ-OH	phenolic OH-group

List of tables

List of figures

Tables

Table 1 – *Main phases in cement ANL and CX from XRD-Rietveld analysis [a]: results obtained with TGA analysis*

Phase composition (mass % of powder)	**ANL**	**CX**
Alite	60.5	54.3
Belite	14.2	18.8
Aluminate cubic	1.3	4.7
Aluminate orthorhombic	0.9	2.4
Ferrite	14.0	6.5
Periclase	0.4	1.1
Quartz	0.3	-
Calcite	3.2/ 3.8 [a]	3.6/ 3.7 [a]
Portlandite	1.1/ 1.4 [a]	2.6/ 2.5 [a]
Anhydrite	-	2.1

Hemihydrate	2.6	1.8
Gypsum	1.0	-
Arcanite		0.6
Aphthitalite	0.4	0.7
Thenardite	-	0.8

1051

1052 Table 2 – *Chemical composition of the cements given by the producers*

Chemical compound (mass % of powder)	**ANL**	**CX**
CaO	62.7	64.0
SiO_2	20.6	20.0
Al_2O_3	4.4	4.6
Fe_2O_3	3.5	2.6
SO_3	3.3	3.6
MgO	1.6	2.4
K_2O	0.4	1.0
Na_2O	0.3	0.2
TiO_2	0.2	0.2
P_2O_5	0.2	0.2
LOI (%) 1000 °C	1.6	1.7
Sum	97.2	98.9

Table 3 - *Physical properties of the materials used*

	ANL	CX	Anhydrite	Hemihydrate	Gypsum
Surface area (BET) (m^2/kg)	890	1330	3000	550	580
Blaine surface (m^2/kg)	360	540			
Density (g/cm^3)	3.1	3.1			
d_{10} (µm)	2.0	2.0			
d_{50} (µm)	12.0	10.0			
d_{90} (µm)	34.0	26.0			

Table 4 - *Chemical and physical properties of LSs*

Mw	g/mol	29000
Mn	g/mol	2100
Organic S ($\propto SO_3$)	mass %	4.6
SO_4^{2-}	mass %	0.9
Ca^{2+}	mass %	4.6
Na^{+}	mass %	0.9
-COOH	mass %	7.1
φ-OH	mass %	1.4
Total sugar	mass %	8.3

1058 Table 5 – *Analysed samples to obtain adsorption isotherms*

Material	LSs addition procedure	LSs dosage (mass % of binder)
ANL cement	IA	0.1; 0.2; 0.4; 0.6; 0.8; 1.2; 1.5; 2.0; 3.0
	DA	0.05; 0.1; 0.25; 0.4; 0.8; 1.2; 1.5
CX cement	IA	0.1; 0.2; 0.4; 0.6; 0.8; 1.0
	DA	0.05; 0.1; 0.2; 0.4; 0.8; 1.2; 1.5

1059 Table 6 – *Mass loss (% dry binder) of ANL and CX cements with increasing amount of LSs*
1060 *added with IA and DA after 30 minutes of hydration. The mass loss is calculated in three*
1061 *temperature intervals: 1: ettringite, calcium sulfates, possibly C-S-H; 2: CH; 3: carbonates.*
1062 *The sum of the mass loss in interval 1 and 2 represents the amount of bound water. *:40-350*
1063 *ºC for CX cement*

Cement type	LSs dosage	Addition procedure	Interval 1 40-300 ºC *	Interval 2 300-500 ºC	Interval 3 500-850 ºC	Bound water 40-500 ºC
			Mass % of dry binder			
ANL	0		2.8	0.6	2.1	3.3
	0.8		2.5	0.4	2.6	3.0
	1.5	IA	3.9	0.8	4.8	4.7
	2.0		2.5	0.6	3.9	3.1
	3.0		3.0	0.7	4.4	3.7
	0.8	DA	2.7	0.2	2.7	2.8
	1.5		2.7	0.7	3.9	3.4

CX	0		2.9	0.8	2.0	3.7
	0.8		4.7	0.9	3.4	5.6
	1.5	IA	6.7	1.0	4.4	7.7
	2.0		5.7	1.0	5.3	6.7
	3.0		4.9	1.0	5.8	5.8
	0.8	DA	2.4	0.8	3.0	3.1
	1.5		2.8	0.9	4.1	3.7

Table 7 – *Summary of the elements detected with XRD in ANL and CX cement pastes with 0/0.8/1.5 mass % of binder LSs (IA) which hydration was stopped after 30 minutes*

Angle 2θ	**Element**	**Symbol in graph**
9.1	Ettringite	AFt
11.6; 20.7	Gypsum	G
12.2; 24.3	C_4AF	F
14.9	C_3S	C_3S
23.0	$CaCO_3$/AFt	Cc/AFt
25.4	Anhydrite	A

Table 8 - *Elemental concentration of Al, Fe, Ca, Si, and S in ANL and CX cements with 0, 0.8 or 1.5 mass % of binder LSs after 30 minutes hydration, and in two LSs solutions (mmol/L): the 2.0 and 3.7 % LSs solutions were used for the cement samples with 0.8 and 1.5 mass % of binder LSs respectively*

Sample	LSs dosage	Al	Ca	Fe	S	Si
	Mass % of binder			Mass %		
ANL IA	0	0.01	24	0	77	0.09
	0.8	0.01	26	0.01	96	0.11
	1.5	0.02	45	0.07	139	0.12
ANL DA	0.8	1.1	38	0.55	100	0.85
	1.5	3.6	52	1.4	72	2.6
CX IA	0	0.01	24	0	176	0.09
	0.8	0.01	10	0.02	169	0.30
	1.5	0.01	54	0.11	141	0.36
CX DA	0.8	0.01	28	0.11	176	0.23
	1.5	0.79	50	0.45	193	0.56
2.0 % LSs sol.		0.02	18	0.02	37	0.31
3.7 % LSs sol.		0.03	32	0.03	66	0.27

Table 9 - *Elemental concentration of Ca and S in the pore solution (mmol/L) of calcium sulfate anhydrous, hemihydrate, and dihydrate, analysed after 30 minutes of hydration, and in two LSs solutions (mmol/L) (2.0 and 3.7 %)*

Sample	**LSs dosage**	**Ca**	**S**
	Mass % of binder	Mass %	
$CaSO_4$	0	34	68
	0.2	38	55
	0.4	36	55
	0.8	30	52
	1.5	30	57
$CaSO_4 \cdot 0.5H_2O$	0	28	74
	0.2	83	93
	0.4	75	86
	0.8	67	83
	1.5	66	85
$CaSO_4 \cdot 2H_2O$	0	20	57
	0.2	30	44
	0.4	42	53
	0.8	63	77
	1.5	72	89

2.0 % LSs sol.	18	37
3.7 % LSs sol.	32	66

Table 10 - *Mass loss (% dry binder) of ANL and CX cements with increasing amount of LSs added with IA and DA after 28 days of hydration. The mass loss is calculated in three temperature intervals: 1: AFt, calcium sulfates, AFm, possibly C-S-H, other hydrates; 2: CH; 3: carbonates. The sum of the mass loss in interval 1 and 2 represents the amount of bound water.*

Cement type	**LSs dosage**	**Addition procedure**	**Interval 1** 40-420 ºC	**Interval 2** 420-540 ºC	**Interval 3** 540-850 ºC
			Mass % of solid		
ANL	0		19.3	5.6	3.8
	0.8	IA	21.0	5.7	4.7
	1.5		22.1	5.7	5.3
	0.8	DA	18.0	5.3	4.0
	1.5		-	-	-
CX	0		21.3	5.8	4.5
	0.8	IA	21.7	5.6	5.2
	1.5		22.4	5.5	5.6
	0.8	DA	21.8	6.0	4.6
	1.5		20.9	5.8	5.5

Table 11 – *Comparison between the amount of LSs that could potentially adsorb in a monolayer on the additional amount of ettringite formed for IA ("calculated Δ"), and the difference in consumed LSs amount experimentally measured between the sample mixed with IA and the one mixed with DA ("measured Δ")*

Cement	**LSs dosage**	**Calculated Δ consumed LSs IA-DA**	**Measured Δ consumed LSs IA-DA**
	mass % of binder	mass % of binder	mass % of binder
ANL	0.8	0.07	0.25
	1.5	0.17	0.72
CX	0.8	0.12	0.16
	1.5	0.18	n.a.

Figures

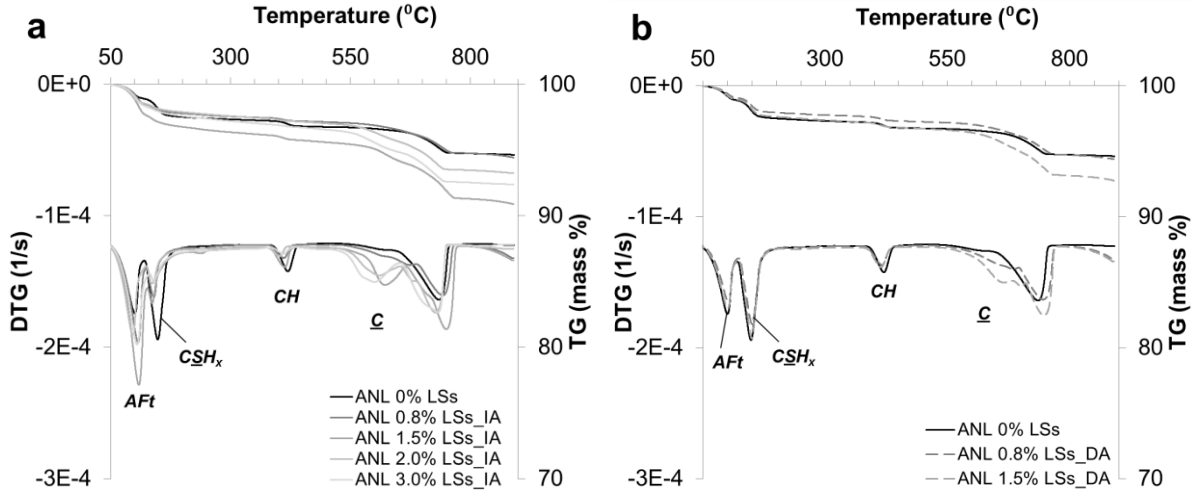

Figure 1 – *TG and DTG curves of ANL cement paste without LSs or a) with 0.8, 1.5, 2.0, 3.0 mass % of binder LSs mixed with IA, or b) with 0.8 and 1.5 mass % of binder LSs mixed with DA. Hydration was stopped after 30 minutes. The peaks corresponding to the decomposition of ettringite (AFt), calcium sulfates ($C\underline{S}H_x$), portlandite (CH) and carbonates ($\underline{C}$) are marked in the figures.*

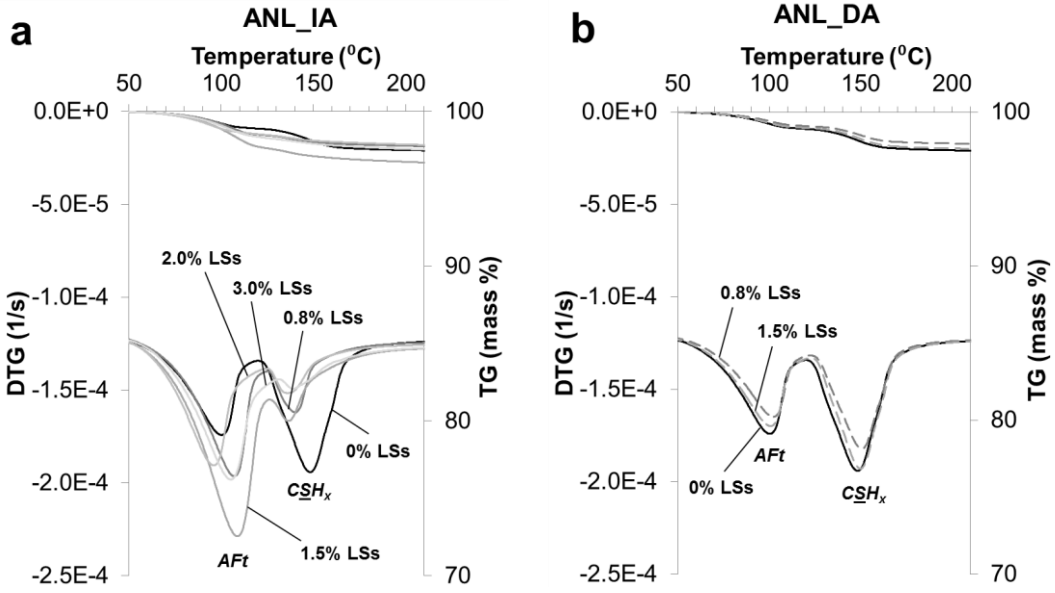

Figure 2 - *TG and DTG curves of ANL cement paste without LSs or with a) 0.8, 1.5, 2.0, 3.0 mass % of binder LSs mixed with IA and b) 0.8, 1.5 mass % of binder LSs mixed with DA , for*

which hydration was stopped after 30 minutes (Part of Figure 1; temperature range: 50-210 ºC). The peaks corresponding to the decomposition of ettringite (AFt) and calcium sulfates ($C\underline{S}H_x$) are marked in the figures.

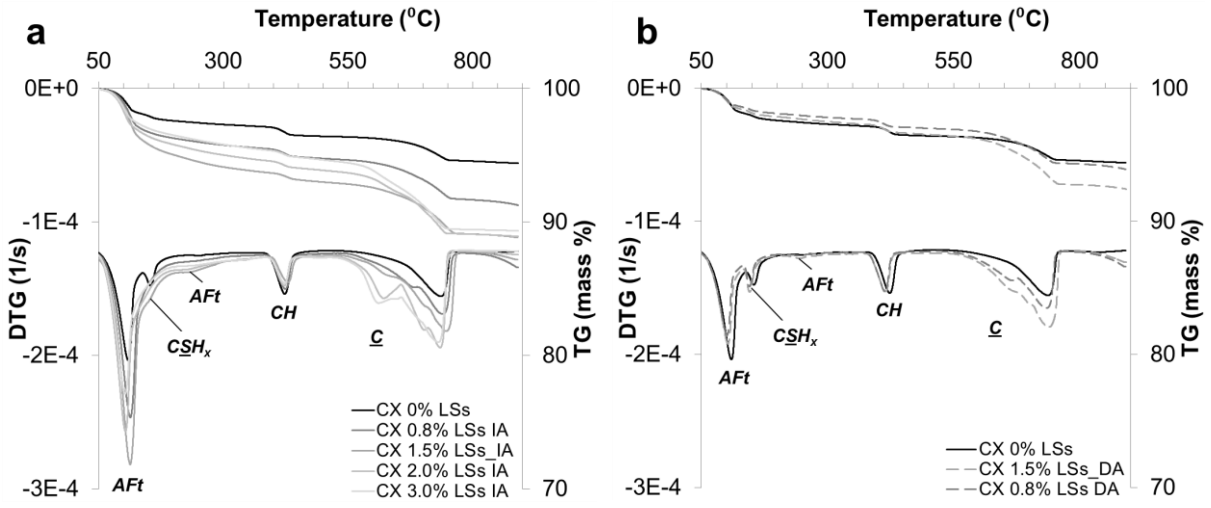

Figure 3 – *TG and DTG curves of CX cement paste without LSs or with 0.8, 1.5, 2.0, 3.0 mass % of binder LSs mixed with a) IA and b) DA, for which hydration was stopped after 30 minutes. The peaks corresponding to the decomposition of ettringite (AFt), anhydrite, hemihydrate or gypsum ($C\underline{S}H_x$), portlandite (CH) and carbonates ($\underline{C}$) are marked in the figures.*

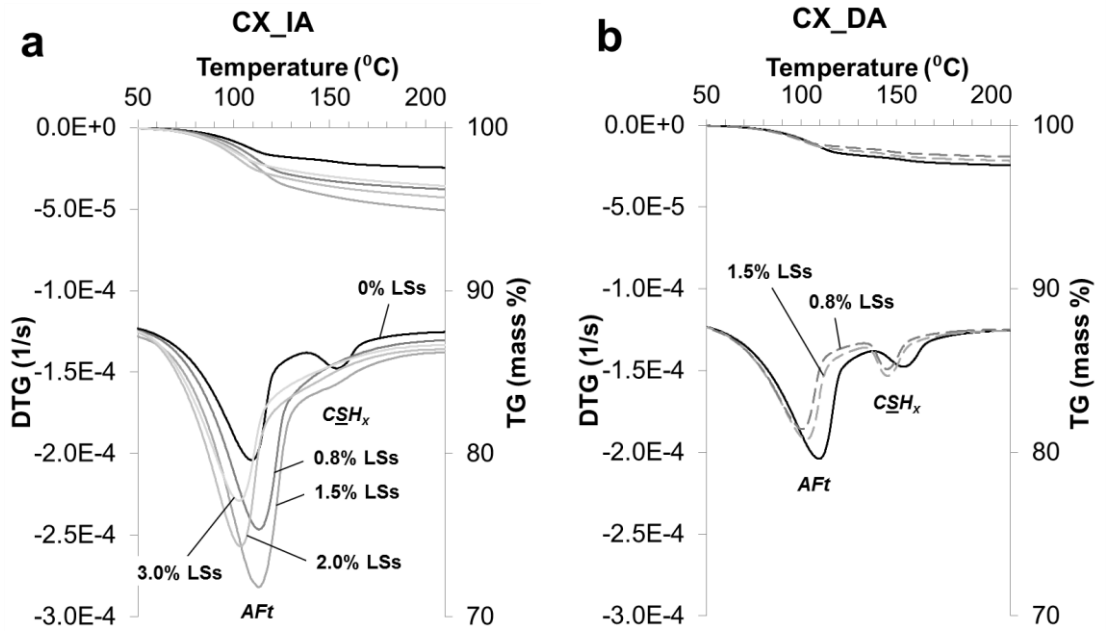

1120

1121 Figure 4 - *TG and DTG curves of CX cement paste without LSs or with a) 0.8, 1.5, 2.0, 3.0*
1122 *mass % of binder LSs mixed with IA and b) 0.8, 1.5 mass % of binder LSs mixed with DA, for*
1123 *which hydration was stopped after 30 minutes (Part of Figure 3; temperature range: 50-210*
1124 *ºC). The peaks corresponding to the decomposition of ettringite (AFt) and calcium sulfates*
1125 *($C\underline{S}H_x$) are marked in the figures.*

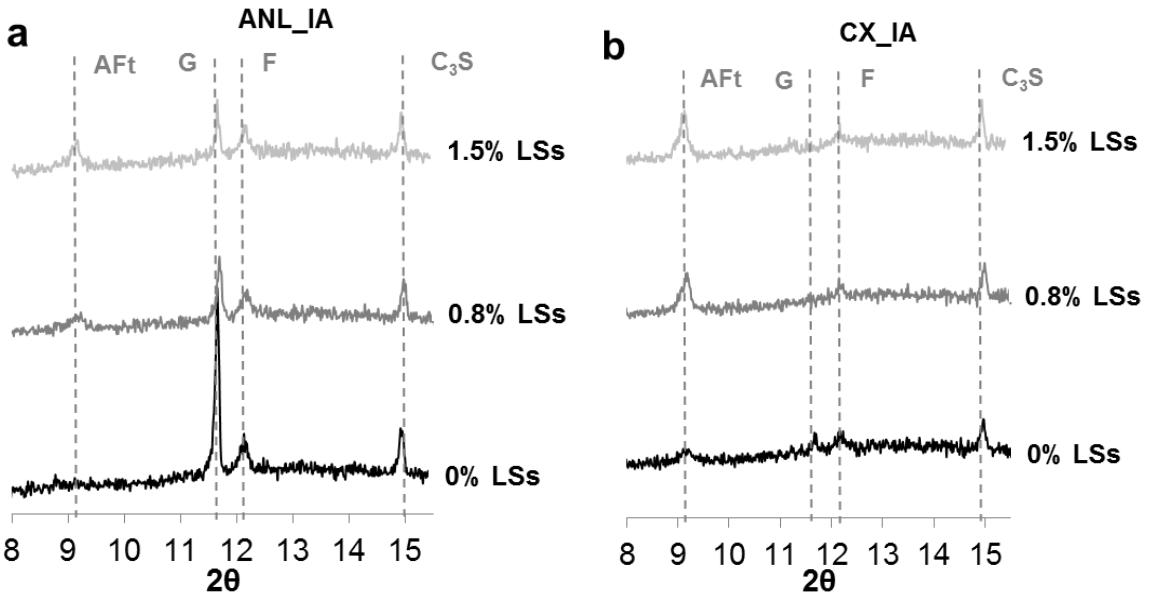

1126
1127 Figure 5 – *X-ray diffraction curves from 2θ = 9 º to 15.5 º for a) ANL and b) CX cement*
1128 *pastes with 0, 0.8, 1.5 mass % of binder LSs (IA) which hydration was stopped after 30*
1129 *minutes. Several peaks are displayed in the figures: AFt: ettringite; G: gypsum; F: C_4AF; C_3S*

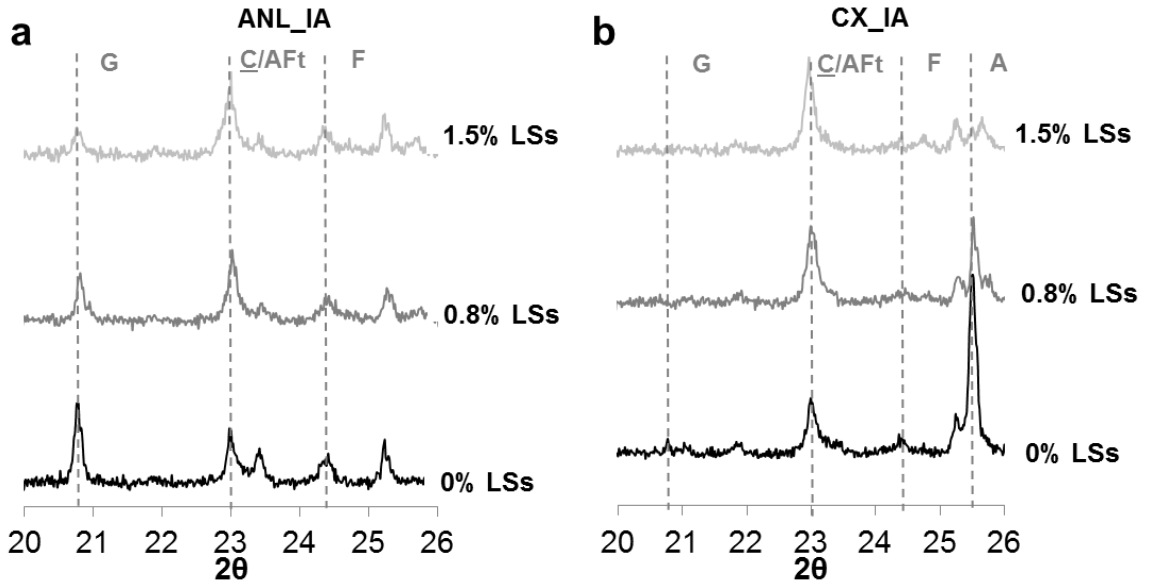

Figure 6 - *X-ray diffraction curves from 2θ = 20 º to 26 º for a) ANL and b) CX cement pastes with 0, 0.8, 1.5 mass % of binder LSs (IA) which hydration was stopped after 30 minutes. Several peaks are displayed in the figures: G: gypsum; C: $CaCO_3$; F: C_4AF; A: anhydrite*

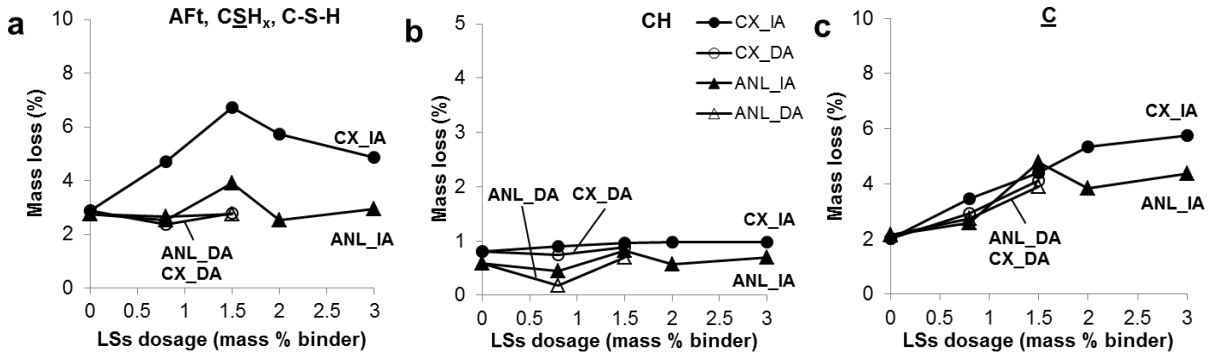

Figure 7 – *Mass loss (% of initial weight) due to a) ettringite (AFt), calcium sulfates (CSH_x), possibly C-S-H; b) CH; c) carbonates (C) vs. LSs dosage (mass % of binder) for ANL and CX cements with increasing amount of LSs added with IA and with DA. The legend in figure b) also applies to figure a) and c). NB. The scale of the y-axis of figure b is different from the one of the other figures.*

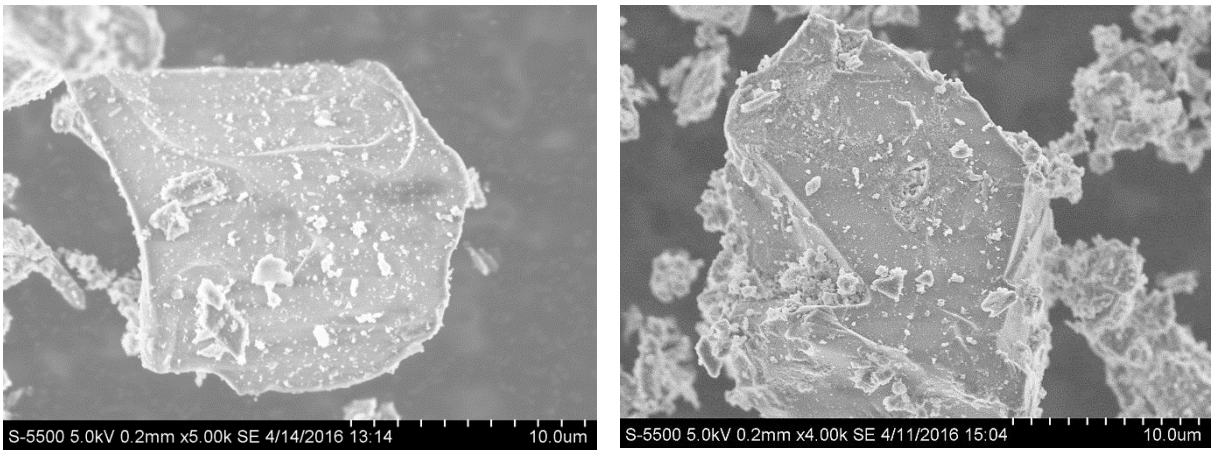

Figure 8 – *SEM images of cement grains of left) ANL and right) CX cement after 30 minutes of hydration without LSs. Width of micrographs: 31 µm*

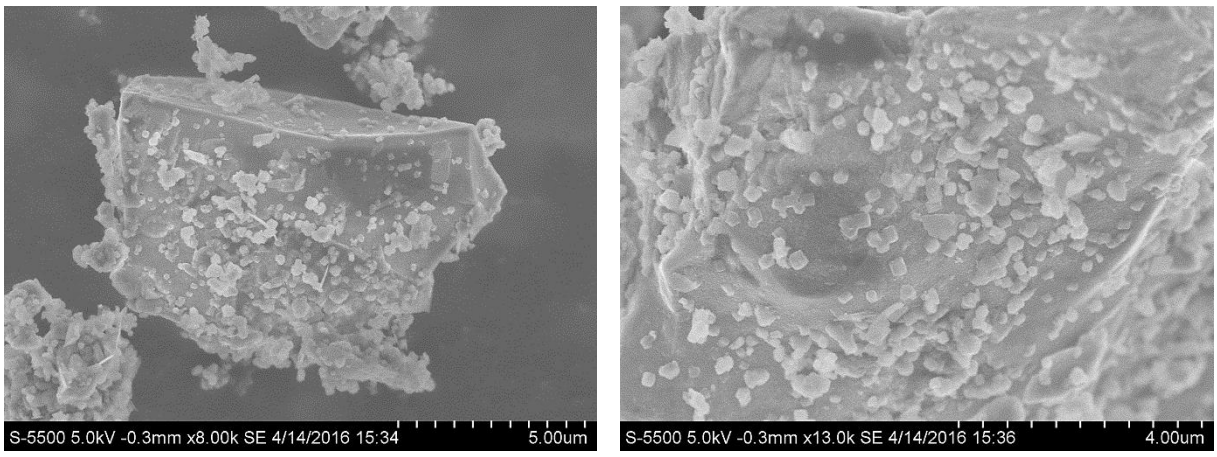

Figure 9 - *SEM images of ANL cement grains after 30 minutes of hydration with 1.5 mass % of binder LSs added with IA. Width of micrograph: left) 16 µm, and right) 10 µm*

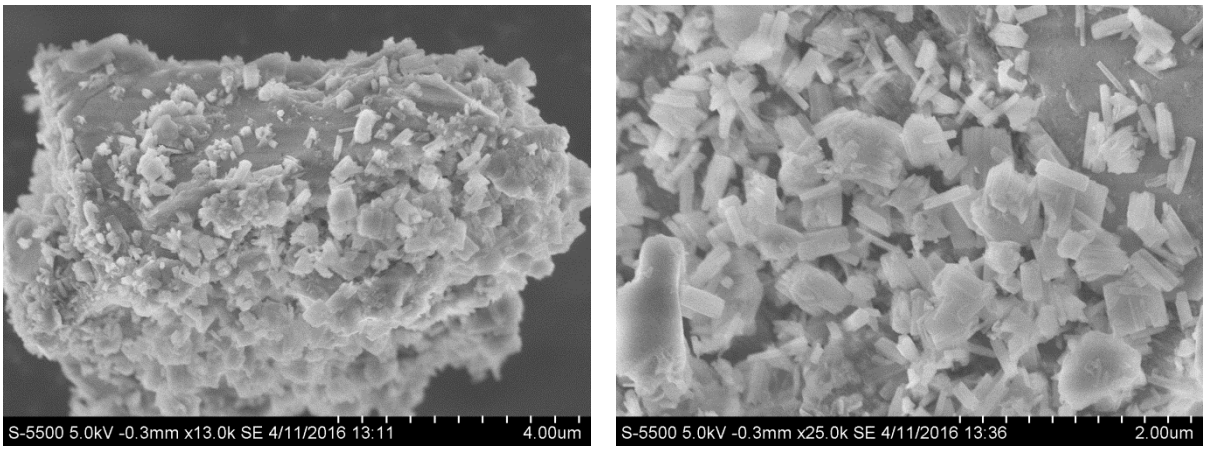

1148

1149 Figure 10 - *SEM images of CX cement grains with 1.5 mass % of binder LSs added with IA*

1150 *after 30 minutes of hydration. Width of micrograph: left) 10 µm, and right) 5 µm*

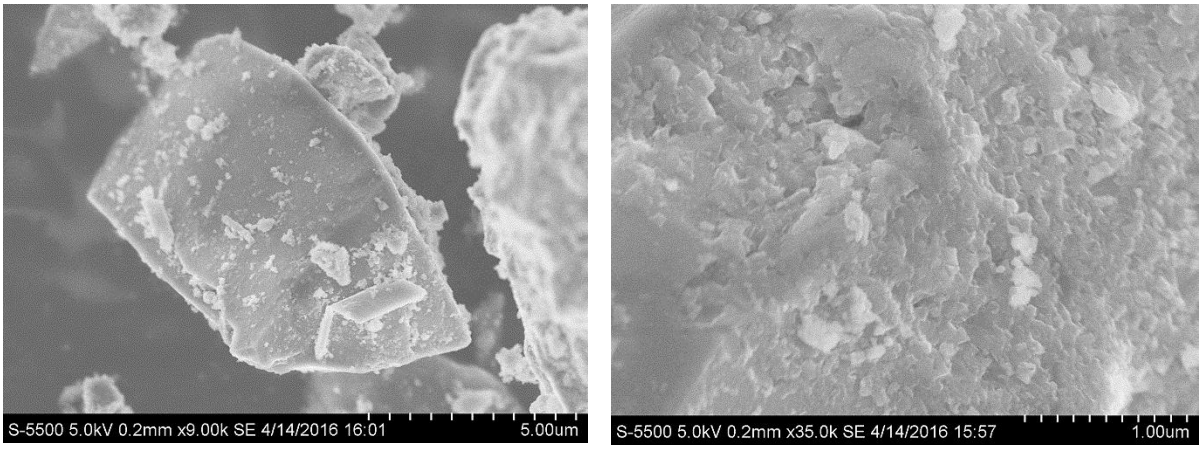

1151

1152 Figure 11 - *SEM images of ANL cement grains with 1.5 mass % of binder LSs added with DA*

1153 *after 30 minutes of hydration. Width of micrograph: left) 14 µm, and right) 4 µm*

1154

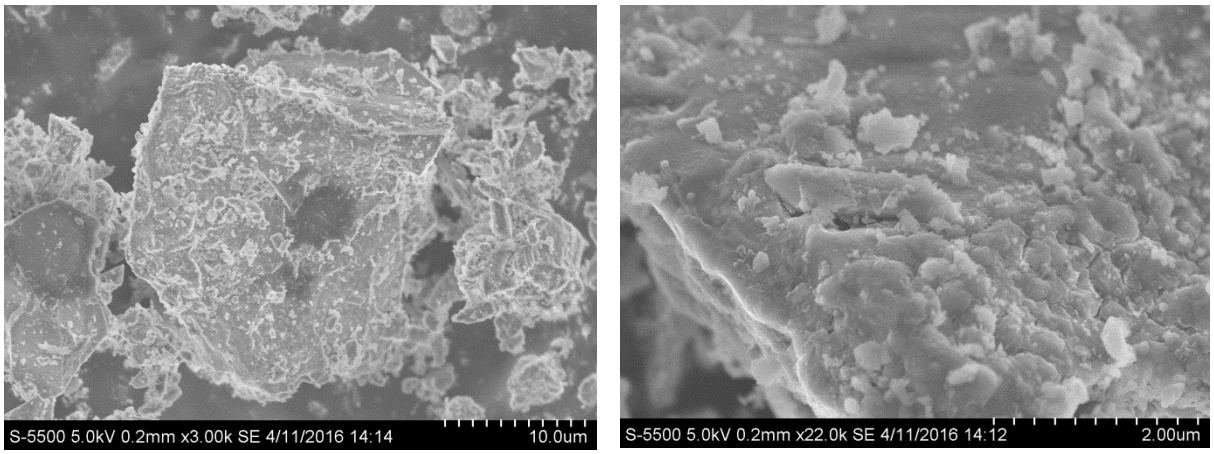

Figure 12 - *SEM images of CX cement grains with 1.5 mass % of binder LSs added with DA after 30 minutes of hydration. Width of micrograph: left) 42 µm, and right) 6 µm*

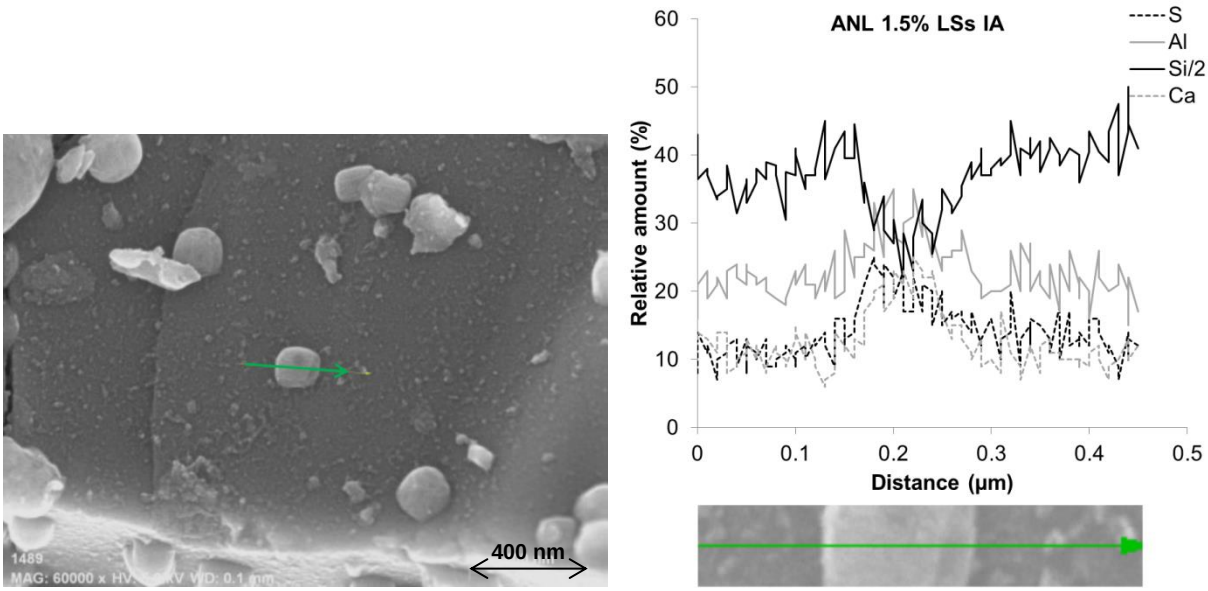

Figure 13 – *Linear SEM-EDS analysis of a crystal on the surface of an unhydrated grain of ANL cement with 1.5 mass % of binder LSs added with IA after 30 minutes of hydration. The crystal analysed is shown in the centre of the micrograph (left; width of micrograph: 2 µm). It has to be noticed that the crystals turned to more rounded shapes during the scanning due to dehydration. The curve representing Si was scaled down by multiplying it by 0.5 for better graphical representation.*

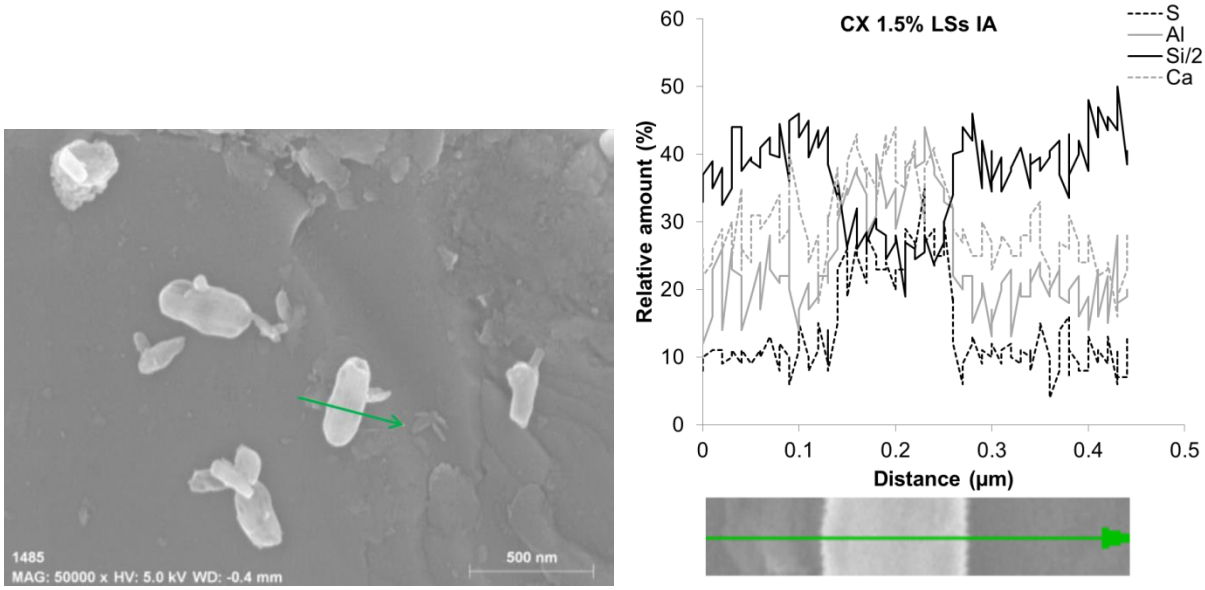

Figure 14 - *Linear SEM-EDS analysis of a crystal on the surface of an unhydrated grain of CX cement with 1.5 mass % of binder LSs added with IA after 30 minutes of hydration. The crystal analysed is shown in the centre of the micrograph (left; width of micrograph: 2.5 µm). It has to be noticed that the crystals turned to more rounded shapes during the scanning due to dehydration. The curve representing Si was scaled down by multiplying it by 0.5 for better graphical representation.*

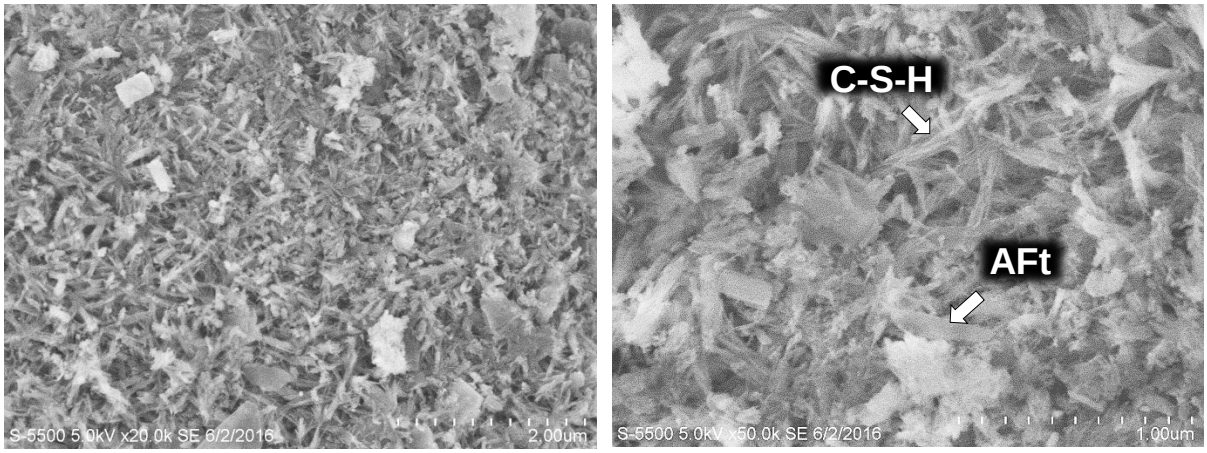

Figure 15 – *SEM images of ANL cement grains without LSs after 6 hours of hydration. Width of micrograph: left) 6 µm, and right) 2.5 µm. The identification of the hydrates (right) was based on visual appearance and comparison to literature, e.g.[33] .*

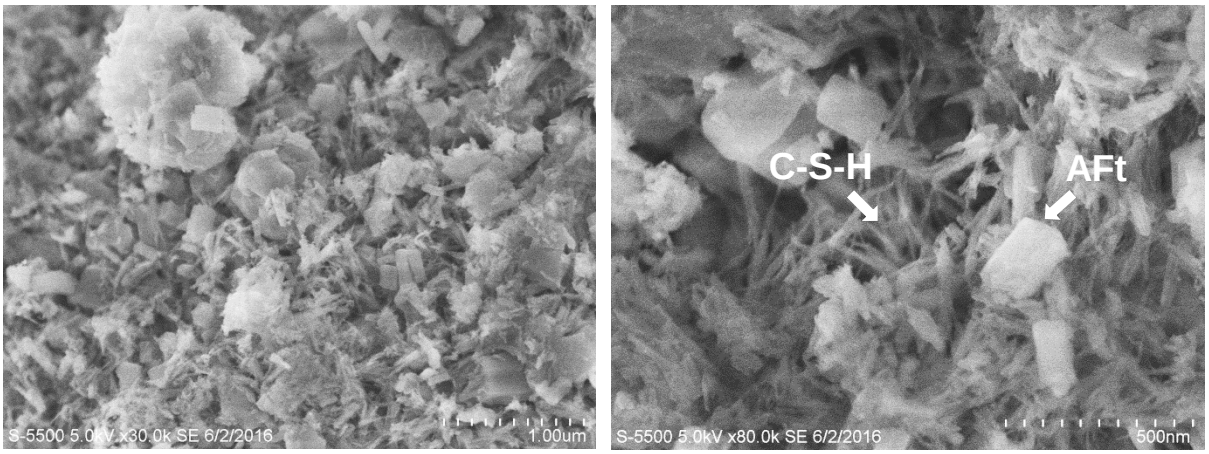

1177

1178 Figure 16 - *SEM images of CX cement grains without LSs after 6 hours of hydration. Width of*

1179 *micrograph: left) 4 µm, and right) 1.6 µm. The identification of the hydrates was based on*

1180 *visual appearance and comparison to literature, e.g. [33].*

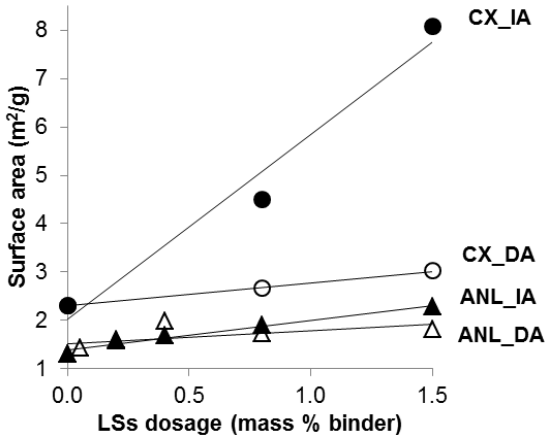

1181

1182 Figure 17 - *Surface area of pastes of ANL and CX cements after 30 minutes of hydration vs.*

1183 *LSs dosage added (mass % of binder) both for IA and DA, after [18]. The specific surface*

1184 *area comprehends the surface area of unhydrated cement grains and hydrates.*

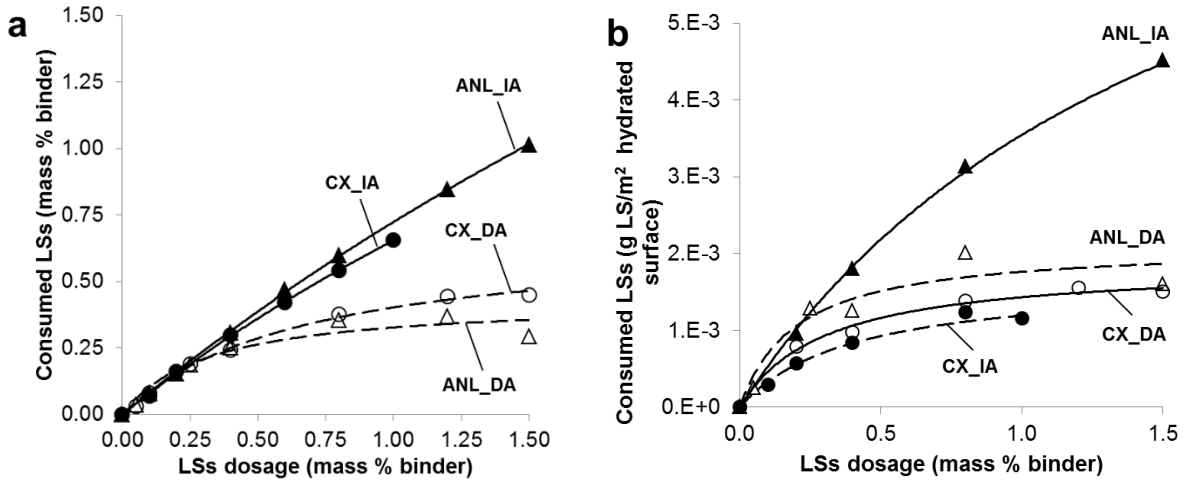

1185

1186 Figure 18 – *Amount of consumed LSs at 30 min. hydration vs. LSs dosage in neat ANL and*
1187 *CX cements for IA and DA, after [18]. The results are calculated as a) mass % of binder and*
1188 *as b) unit of surface area available for adsorption of hydrated pastes of ANL and CX cements*

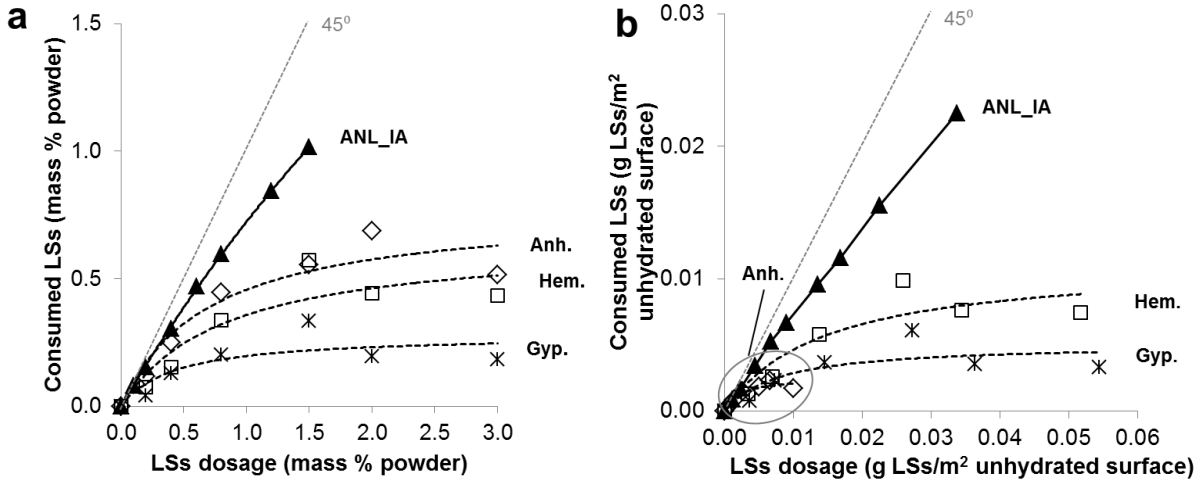

1189

1190 Figure 19 - *Amount of consumed LSs at 30 min. hydration vs. LSs dosage added to calcium*
1191 *sulfate anhydrous (anh.), hemihydrate (hem) and dihydrate (gyp.) for IA. The results are*
1192 *calculated as a) mass % of powder, and b) g LSs/m^2 unhydrated surface*

1193

1194

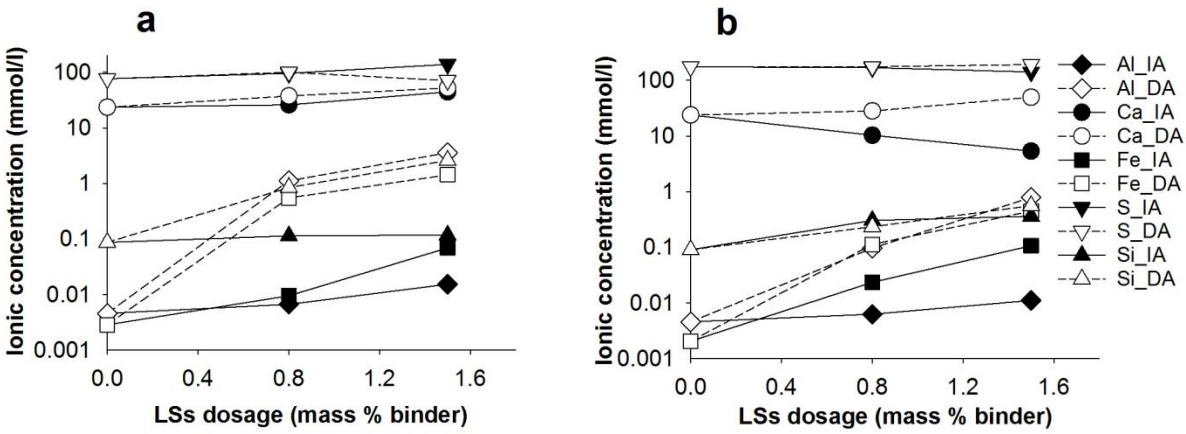

1195

1196 Figure 20 – *Concentration of Al, Fe, Ca, Si, and S in the pore solution (mmol/l) expressed in*
1197 *logarithmic scale vs. total LSs added (mass % of binder) to a) ANL and b) CX cement pastes*
1198 *analysed after 30 minutes of hydration both for IA and DA. The legend in figure b) also*
1199 *applies to figure a).*

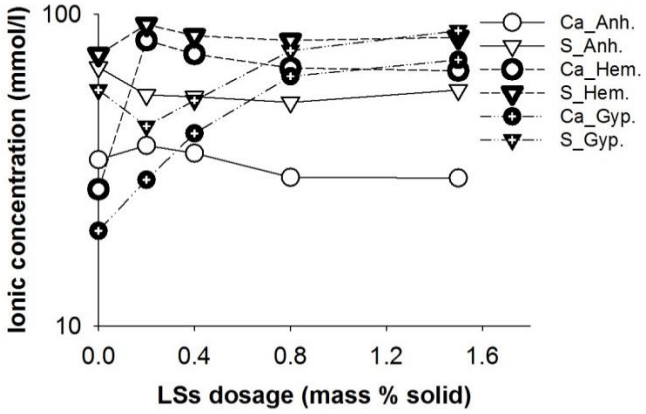

1200

1201 Figure 21 - *Concentration of Ca and S in the pore solution (mmol/l) expressed in logarithmic*
1202 *scale vs. total LSs added (mass % of powder) with IA to calcium sulfate anhydrous,*
1203 *hemihydrate, and dihydrate, analyzed after 30 minutes of hydration*

1204

1205

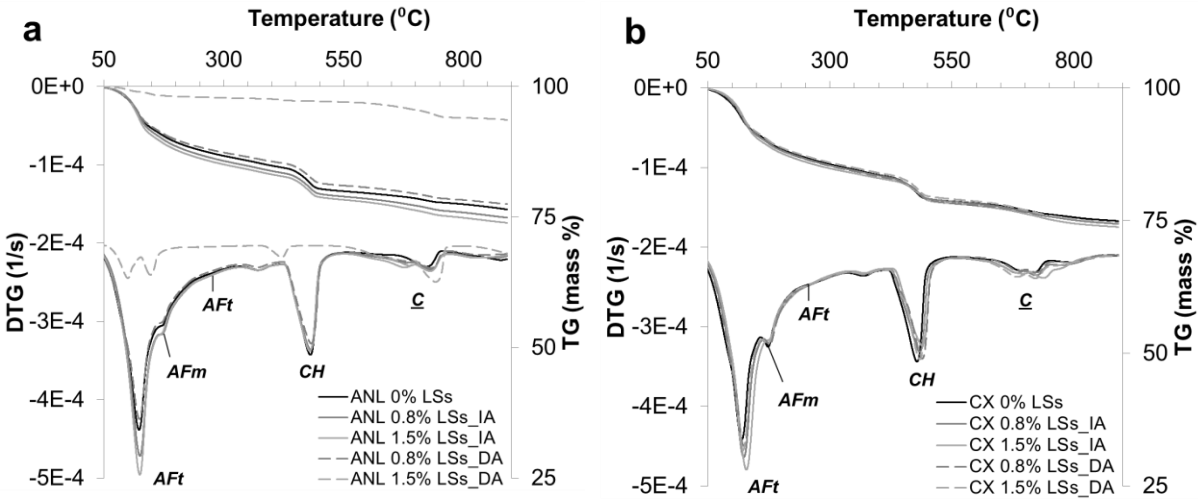

Figure 22 - *TG and DTG curves of a) ANL and b) CX cement paste without LSs or with 0.8, 1.5, 2.0, 3.0 mass % of binder LSs mixed with IA and DA, for which hydration was stopped after 28 days. The peaks corresponding to the decomposition of AFt, AFm, portlandite (CH) and carbonates (C) are marked in the figures.*

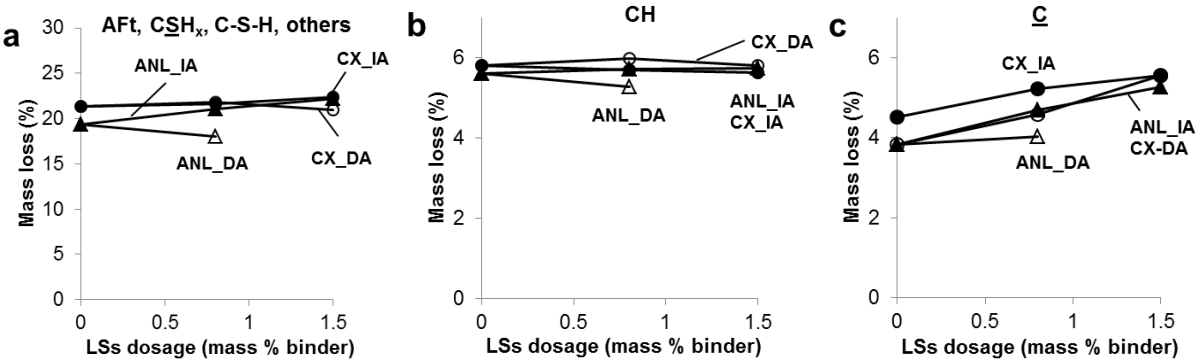

Figure 23 – M*ass loss (% of initial weight) of a) AFt, calcium sulfate hydrates (CSH$_x$), AFm, C-S-H; b) CH; c) carbonates (C)vs. LSs dosage (mass % of binder) for ANL and CX cements with increasing amount of LSs added with IA and with DA. NB. The scale of the y-axis of figure a) is different than the one of the other figures.*

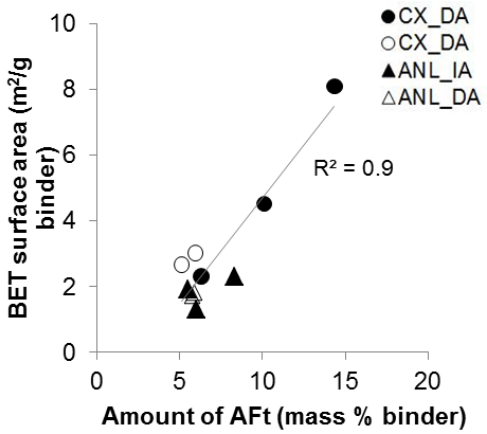

1219

1220 Figure 24 - *Correlation between the calculated amount of ettringite* and the particle surface*
1221 *area of solids in pastes of the two cements when LSs was added immediately with the mixing*
1222 *water (IA). *: Amount of ettringite calculated considering the mass loss in the whole interval*
1223 *1 (50 - ca. 300 ºC)*